Pediatr Blood Cancer 2010;54:329–331

BRIEF REPORT
Successful Treatment of Refractory Donor Lymphocyte Infusion-Induced Immune-Mediated Pancytopenia with Rituximab

Itaru Kato, MD,[1] Katsutsugu Umeda, MD,[1]* Tomonari Awaya, MD,[1] Yoshihiro Yui, MD,[1] Akira Niwa, MD,[1] Hisanori Fujino, MD,[1] Hiroshi Matsubara, MD,[1] Ken-Ichiro Watanabe, MD,[1] Toshio Heike, MD,[1] Naoto Adachi, MD,[2] Fumio Endo, MD,[2] Tomoyuki Mizukami, MD,[3] Hiroyuki Nunoi, MD,[3] Tatsutoshi Nakahata, MD,[1] and Souichi Adachi, MD[1]

A 6-year-old male with chronic granulomatous disease, who was transplanted with bone marrow and exhibited increasing mixed chimerism, subsequently received two donor lymphocyte infusions (DLI). Two weeks after the second DLI, the patient developed acute graft-versus-host disease (GVHD) and progressive pancytopenia that was associated with autoantibody production. Conventional treatment did not improve the pancytopenia. However, administration of Rituximab (RTX) (375 mg/m^2/week for four consecutive weeks) resulted in a rapid resolution of the pancytopenia. The patient achieved full donor chimerism without GVHD symptoms. RTX can be valuable for managing immune-mediated cytopenias that arise after DLI and are refractory to conventional therapies. Pediatr Blood Cancer 2010;54:329–331. © 2009 Wiley-Liss, Inc.

Key words: allogeneic stem cell transplantation; antibodies; graft rejection; graft-versus-host disease; immune responses; Rituximab

INTRODUCTION

Donor leukocyte infusion (DLI) is used as an immunotherapy not only for preventing the reemergence of malignancies, but also for preventing graft rejection after allogeneic hematopoietic stem cell transplantation (hSCT) that results in the development of mixed increasing chimerism [1]. However, DLI treatment is also associated with substantial toxicity. For example, it has been shown that up to 41% of patients receiving DLI suffer from myelosuppression, which could lead to death from causes other than the underlying disease [2,3]. Like the cytopenias associated with graft-versus-host disease (GVHD), the cytopenias that can arise after DLI are conventionally treated by steroids, intravenous immunoglobulin (IVIG), and splenectomy. However, the prognosis of cases that are refractory to conventional treatments remains dismal as the treatment of such cases has not been established. Anti-CD20 antibody (Rituximab, RTX), a humanized murine monoclonal antibody that is often used to treat B-cell malignancies, has been shown to effectively treat various autoimmune diseases that arise after hSCT [4–6]. Here, we describe a patient with severe immune-mediated pancytopenia after DLI who responded well to RTX therapy.

CASE REPORT

A 4-month-old male was diagnosed with X-linked chronic granulomatous disease on the basis of his reduced NADPH oxidase levels (<5%) and the complete absence of gp91-phox. Despite prophylactic treatment with trimethoprim–sulfamethoxazole and itraconazole, and interferon-γ, he suffered repeatedly from severe bacterial and fungal infections, including multiple episodes of pulmonary aspergillosis. Therefore, allogeneic hSCT was planned, and the patient was transferred at 6 years of age to our hospital for bone marrow transplantation (BMT) from a genotypically HLA-matched, blood-type compatible unrelated donor. The HLA type of the donor and the patient was HLA-A 33/24, -B 58/52, -DR 1302/1502. The conditioning regimen included fludarabine 30 mg/m^2/day for 6 days from day −7 to −2, cyclophosphamide 30 mg/kg/day for 4 days from day −6 to −3, anti-T lymphocyte globulin 2.5 mg/kg/day for 4 days from day −6 to −3, and total body irradiation 300 cGy on day −1. To prevent GVHD, the patient received tacrolimus and short-methotrexate (day 1: 10 mg/m^2, day 3.6: 7 mg/m^2), as previously reported [7]. Subsequently, 4.8×10^8/kg mononucleated cells were infused without T-cell depletion. The patient's bone marrow (BM) was analyzed serially for chimerism by microsatellite PCR, and the presence of oxidase-positive neutrophils in the peripheral blood (PB) was determined by fluorescence-activated cell sorting using a dihydrorhodamine oxidation assay. Hematopoietic engraftment occurred rapidly. The neutrophil count exceeded 0.5×10^9/L on day 10, the reticulocyte count exceeded 10‰ on day 17, and the platelet counts did not drop below 40×10^9/L during this period. However, the donor chimerism of the patient was unstable. After the dosage of tacrolimus was reduced on day 25, grade II acute GVHD of the skin developed on day 37, which was resolved by a short course of prednisolone (PSL) treatment. Subsequently, the patient achieved full donor chimerism of BM on day 61, and the oxidase-positivity of PB neutrophils was 100% on day 82. The GVHD did not worsen after treatment with PSL and tacrolimus was discontinued on days 98 and 361, respectively.

Although the patient was asymptomatic and there were no abnormal laboratory findings, the oxidase-positivity of PB neutrophils gradually decreased to 50% and 13% on days 404 and 758,

[1]Department of Pediatrics, Graduate School of Medicine, Kyoto University, Kyoto, Japan; [2]Department of Pediatrics, Graduate School of Medicine, Kumamoto University, Kumamoto, Japan; [3]Faculty of Medicine, Department of Pediatrics, University of Miyazaki, Miyazaki, Japan

The authors declare no competing financial interests.

*Correspondence to: Katsutsugu Umeda, Department of Pediatrics, Graduate School of Medicine, Kyoto University, 54, Kawahara-cho, Shogoin, Sakyo-ku, Kyoto 606-8507, Japan.
E-mail: umeume@kuhp.kyoto-u.ac.jp

Received 1 May 2009; Accepted 10 August 2009

DOI 10.1002/pbc.22280
Published online 3 November 2009 in Wiley InterScience (www.interscience.wiley.com)

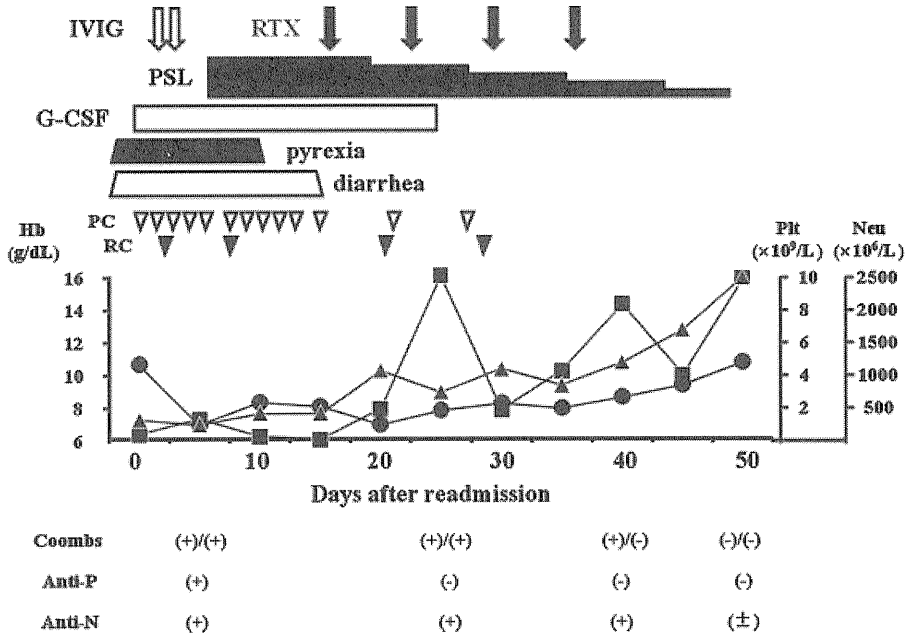

Fig. 1. The clinical course after readmission. IVIG, intravenous immunoglobulin; RTX, Rituximab; PSL, prednisolone; G-CSF, granulocyte colony-stimulating factor; RC, packed red blood cell concentrate; PC, packed platelet concentrate; Plt, platelet counts; Neu, neutrophil counts; Coombs, direct/indirect Coombs test; Anti-P, anti-platelet antibody; Anti-N, anti-neutrophil antibody. Closed circles, triangles, and squares indicate Hb levels, platelet counts (Plt), and neutrophil counts (Neu), respectively.

respectively. In an attempt to induce his return to full donor chimerism, the patient was given frozen 1.0×10^7 and 5.0×10^7 PB lymphocytes/kg on days 805 and 850, respectively, which had been harvested from the same donor who had provided the BM. Before this second DLI, the patient had not undergone any notable events such as contracting an infectious disease, medication changes or vaccinations. The clinical course after the second DLI is shown in Figure 1. Two weeks after it was delivered, the patient developed a skin rash, diarrhea, fever, elevated serum liver enzyme value, and thrombocytopenia. The patient was diagnosed clinically as having GVHD. Since restarting the patient on tacrolimus did not improve his symptoms, he was readmitted to our hospital on day 44 after the second DLI.

On readmission, the physical examination revealed no abnormal symptoms except for a persistent high fever. The results of the laboratory investigations are shown in Table I. Antibody screening tests revealed strong positivity in the direct and indirect Coombs test, and the presence of anti-platelet antibodies and anti-neutrophil antibodies specific for HNA-1a and 1b. However, other antibody screening tests were negative. There was no fungal infection or recurrence of CMV and EBV. An examination of the BM on day 896 after the BMT revealed a hypocellular marrow, but no

TABLE I. Laboratory Data on Readmission

	Value	Unit	Normal range		Value	Unit	Normal range		Value	Normal range
WBC	3.1	10^9/L	3.6–9.8	AST	38	IU/L	13–33	CMVpp65	(−)	(−)
Neu	0.93	10^9/L	1.6–6.0	ALT	36	IU/L	8–42	EBV-DNAPCR	(−)	(−)
Lymph	2.2	10^9/L	1.1–3.9	LDH	273	IU/L	129–241	Aspergillus-Ag	(−)	(−)
Hb	10.6	g/dl	11.3–13.7	ALP	473	IU/L	115–359	Candida-Ag	(−)	(−)
Reti	7.1	10^9/L	2.7–9.3	T.Bil	0.8	mg/dl	0.3–1.3	Direct Coombs Test	(+)	(−)
Plt	12	10^9/L	192–456	TP	7.3	mg/dl	6.3–8.1	Indirect Coombs Test	(+)	(−)
Haptoglobin	102.4	mg/dl	14–294	Alb	4.3	mg/dl	3.9–5.1			
CRP	4.9	mg/dl	<0.2	Soluble IL2	972	U/ml	145–519	Anti-neutrophil antibodies	(+)	(−)
β-DG	7.473	ng/ml	<11	Ferritin	7.3	ng/ml	<155	Anti-HNA-a	(+)	(−)
Endotoxin	<1.76	pg/ml	<5	Triglycerides	58	mg/dl	34–173	Anti-HNA-b	(+)	(−)
								Anti-platelet antibodies	(+)	(−)

WBC, white blood cell; Neu, neutrophil; Lymph, lymphocyte; Hb, hemoglobin; Reti, reticulocyte; Plt, platelet; CRP, C-reactive protein; β-DG, β-D-glucan; AST, aspartate aminotransferase; ALT, alanine aminotransferase; LDH, lactate dehydrogenase; ALP, alkaline phosphatase; T.Bil, total bilirubin; TP, total protein; Alb, albumin; CMVpp65, Cytomegalovirus pp65; EBV, Epstein–Barr virus; Ag, antigen; HNA, human neutrophil antigen.

evidence of malignancy or hemophagocytosis. Chimerism studies of the BM revealed 55% of the cells were composed of donor cells. Only 17% of the PB neutrophils were oxidase-positive. The patient was first treated with IVIG (1 g/kg/day for 2 days), PSL (2 mg/kg/day daily), and granulocyte colony-stimulating factor (G-CSF). Although this initial treatment resolved the pyrexia and diarrhea, the patient's pancytopenia gradually progressed and multiple transfusions became necessary. Given his refractory autoimmune pancytopenia, he was treated with RTX (375 mg/m^2/week for four consecutive weeks). The neutrophil counts rose markedly within a few days after the first RTX infusion, which was followed by the gradual increase in Hb and platelet counts. The patient became transfusion-independent after the third RTX course, and pancytopenia did not recur when the patient stopped receiving G-CSF and PSL. The hematological values normalized 21 days after the initial RTX infusion. The autoimmune antibody levels dropped during RTX treatment and eventually disappeared almost completely. Both BM chimerism studies and analysis of the oxidase-positivity of the PB neutrophils revealed 100% donor chimerism 80 days after the initial RTX infusion. Three years after the RTX treatment, the patient was alive and free of disease and showed no signs of mixed chimerism or GVHD.

DISCUSSION

Cytopenias that follow allogeneic hSCT can be immune-mediated and are frequently associated with GVHD. Autoimmune hemolytic anemia (AIHA) and immune thrombocytopenia (ITP) occur frequently, but immune-mediated cytopenias, including autoimmune neutropenia (AIN), are relatively rare [4,5]. Cytopenias are also often seen in patients after DLI and are thought to be mediated by autoimmune mechanisms, as with GVHD. In our case, pancytopenia developed soon after DLI, along with acute GVHD and the emergence of autoantibodies against multilineage blood cells. Notably, the levels of these antibodies decreased in parallel with the improvement of the pancytopenia, while the blood and BM analyses suggested that other possible causes of cytopenias, such as viral infections and hemophagocytic histiocytosis, were unlikely. However, the BM examination also showed a hypocellular marrow, which suggested that the pancytopenia did not arise from antibody-mediated cell destruction alone. Our findings suggest that autoimmunity was the major cause of the severe pancytopenia exhibited by our patient.

Most patients with autoimmune cytopenias are rescued by the administration of high-dose IVIG and standard immunosuppressive agents such as steroids [8,9]. Furthermore, RTX has been demonstrated to be useful for treating the AIHA and ITP that follow GVHD, which is refractory to conventional treatment [5,6,10–13]. However, the prognosis of patients who develop autoimmune pancytopenia remains to be determined. Page et al. [4] reported two cases that developed pancytopenia after umbilical cord blood transplantation. Despite receiving immunosuppressive treatment, including RTX, one patient continued to need the therapy while the other required a second transplantation because of pancytopenia.

Despite the fact that our patient was initially treated with PSL, high-dose IVIG, and G-CSF, and showed improvements in the other symptoms of acute GVHD, his pancytopenia progressed. Given this rapid and potentially fatal progression, we chose to start a salvage therapeutic approach rather than continue such conventional treatments, which would result in a slower response. The institution of RTX resulted in the resolution of the pancytopenia and the almost complete disappearance of the autoimmune antibodies. Furthermore, the response to RTX was already obvious 1 week after the first RTX infusion, which is consistent with a study that showed that RTX induces a prompt response in a subpopulation of patients [14].

Although no definite conclusions can be drawn from a single case with a relatively short period of follow-up, this case strengthens the hypothesis that RTX can be a beneficial treatment for refractory DLI-induced immune-mediated pancytopenia. This case suggests that further clinical research examining the merits of RTX in such cases is warranted.

REFERENCES

1. Slavin S, Morecki S, Weiss L, et al. Donor lymphocyte infusion: The use alloreactive and tumor-reactive lymphocytes for immunotherapy of malignant and nonmalignant diseases in conjunction with allogeneic stem cell transplantation. J Hematother Stem Cell Res 2002;11:265–276.
2. Kolb HJ, Schattenberg A, Goldman JM, et al. Graft-versus-leukemia effect of donor lymphocyte transfusions in marrow grafted patients. Blood 1995;86:2041–2050.
3. Collins RHJR, Shpiberg O, Drobyski WR, et al. Donor leukocyte infusions in 140 patients with relapsed malignancy after allogeneic bone marrow transplantation. J Clin Oncol 1997;15:433–444.
4. Page KM, Mendizabal AM, Prasad VK, et al. Posttransplant autoimmune hemolytic anemia and other autoimmune cytopenias are increased in very young infants undergoing unrelated donor umbilical cord blood transplantation. Biol Blood Marrow Transplant 2008;14:1108–1117.
5. Raj K, Narayanan S, Auguston B, et al. Rituximab is effective in the management of refractory autoimmune cytopenias occurring after allogeneic stem cell transplantation. Bone Marrow Transplant 2005;35:299–301.
6. Zaja F, Bacigalupo A, Patriaca F, et al. Treatment of refractory chronic GVHD with rituximab: A GITMO study. Bone Marrow Transplant 2007;40:273–277.
7. Kojima S, Matsuyama T, Kato S, et al. Outcome of 154 patients with severe aplastic anemia who received transplants from unrelated donors: The Japan Marrow Donor Program. Blood 2002;100:799–803.
8. Cines DB, Bussel JB. How I treat idiopathic thrombocytopenic purpura (ITP). Blood 2005;106:2244–2251.
9. Gehrs BC, Friedberg RC. Autoimmune hemolytic anemia. Am J Hematol 2002;69:258–271.
10. Stasi R, Pagano A, Stipa E, et al. Rituximab chimeric CD20 antibody treatment for adults with chronic idiopathic thrombocytopenic purpura. Blood 2001;98:952–957.
11. Ratanatharathorn V, Carson E, Reynolds C, et al. Anti-CD20 chimeric monoclonal antibody treatment of refractory immune-mediated thrombocytopenia in a patient with chronic graft-versus-host disease. Ann Intern Med 2000;133:275–279.
12. Hongeng S, Tardong P, Worapongpaiboon S, et al. Successful treatment of refractory autoimmune hemolytic anaemia in a post-unrelated bone marrow transplant paediatric patient with Rituximab. Bone Marrow Transplant 2002;29:871–872.
13. Corti P, Bonanimi S, Vallinoto C, et al. Rituximab for immune hemolytic anaemia following T and B cell depleted hematopoietic stem cell transplantation. Acta Haematol 2003;109:43–45.
14. Mohty M, Marchetti N, El-Cheikh J, et al. Rituximab as salvage therapy for refractory chronic GVHD. Bone Marrow Transplant 2008;41:909–911.

TABLE 2 Details of response to sequential treatments where applicable ($n = 10$)

No.	Severity of disease	First treatment		Second treatment		Third treatment	
1	Severe	Amlodopine	×	Nifedipine	√	–	–
2	Moderate	Amlodopine	×	GTN	×	–	–
3	Moderate	Amlodopine	×	GTN	×	–	–
4	Severe	Nifedipine	×	Amlodopine	×	–	–
5	Severe	Nifedipine	×	Amlodopine	×	GTN	√
6	Moderate	Nifedipine	×	GTN	×	–	
7	Severe	GTN	×	Amlodopine	×	Nifedipine	√
8	Moderate	Nifedipine	×	GTN	√	–	–
9	Severe	Amlodopine	×	Nifedipine	×	GTN	×
10	Moderate	Amlodopine	√	GTN	√	–	–

×: no response/inadequate response; √: response.

Overall, GTN patches were effective in 55% of the treated patients. Efficacy was better than that of nifedipine and amlodipine (33 *vs* 25% response rate, respectively), but small numbers and retrospective analysis does not allow statistical comparison. Response was similar in primary and secondary RP. Children with severe RP had a better response to nifedipine and amlodopine than children with moderate disease. The sub-group with severe disease was more likely to be using a disease-modifying drug, which may have had an impact. However, numbers are too small for any conclusion to be drawn from this.

Application of GTN patches allows removal if adverse events occur. Together with absence of tablets, this may make treatment with GTN attractive in paediatric practice. All patients received Deponit GTN patches. Alternative brands may not have adequate skin adhesion when cut into quarters for this off-license use.

GTN patches, nifedipine and amlodipine offer symptomatic relief for patients with moderate primary/secondary RP. Further studies, including head-to-head trials, are needed to determine if one agent is superior. Meanwhile, GTN patches offer an alternative to oral calcium channel blockers for symptomatic relief of paediatric RP.

Rheumatology key message

- GTN patches are an efficacious treatment option in paediatric RP.

Disclosure statement: The authors have declared no conflicts of interest.

Kapil Gargh[1], Eileen M. Baildam[1], Gavin A. Cleary[1], Michael W. Beresford[1] and Liza J. McCann[1]

[1]*Department of Paediatric Rheumatology, Alder Hey Children's NHS Foundation Trust, Liverpool, UK*
Accepted 20 August 2009
Correspondence to: Liza McCann, Department of Paediatric Rheumatology, Alder Hey Children's NHS Foundation Trust, Eaton Road, Liverpool, L12 2AP, UK.
E-mail: liza.mccann@alderhey.nhs.uk

References

1 Anderson ME, Moore TL, Hollis S, Jayson MIV, King TA, Herrick AL. Digital vascular response to topical glyceryl trinitrate, as measured by laser Doppler imaging, in primary Raynaud's phenomenon and systemic sclerosis. Rheumatology 2002;41:324–28.

2 Franks AG Jr. Topical glyceryl trinitrate as adjunctive treatment in Raynaud's disease. Lancet 1982;1:76–7.

3 Teh LS, Mannig J, Moore T, Tully MP, O'Reilly D, Jayson MIV. Sustained-release transdermal glyceryl trinitrate patches as a treatment for primary and secondary Raynaud's phenomenon. Br J Rheumatol 1995; 34:636–41.

4 Nigrovic PA, Fuhlbrigge RC, Sundel RP. Raynaud's phenomenon in children: a retrospective review of 123 patients. Pediatrics 2003;111:715–21.

5 Coppock JS, Hardman JM, Bacon PA, Woods KL, Kendall MJ. Objective relief of vasospasm by glyceryl trinitrate in secondary Raynaud's phenomenon. Postgrad Med J 1986;62:8–15.

Rheumatology 2010;49:194–196
doi:10.1093/rheumatology/kep315
Advance Access publication 23 October 2009

A case of early-onset sarcoidosis with a six-base deletion in the *NOD2* gene

SIR, We present the first case of early-onset sarcoidosis (EOS, MIM no. 609464) with a six-base deletion in the *NOD2* gene, resulting in the replacement of one amino acid and the deletion of two additional amino acids. All previous mutations reported for EOS and Blau syndrome (BS, MIM no. 186580) were single-base substitutions that resulted in the replacement of a single amino acid [1–3].

The patient was a Japanese male born after an uncomplicated pregnancy and delivery. His family had no symptoms of skin lesions, arthritis or uveitis. At 5 years of age, he was diagnosed with bilateral severe uveitis. He became blind in both eyes during adolescence. He had swollen ankles without pain during childhood,

and developed arthritis in his both knees and ankles at 15 years of age. At 30 years, a skin rash had developed on his extremities after his first BCG vaccination. The skin lesions were scaly erythematous plaques with multiple lichenoid papules and some pigmentation. At the same age, camptodactyly without obvious synovial cysts of the hands was observed, and the deformity in all fingers developed by 35 years. At 41 years, he had low-grade fever for 1 year. He had no pulmonary lesions. His laboratory investigations showed normal white blood cell count, mildly elevated CRP (1.0 mg/dl) and ESR (20 mm/h). A skin biopsy from his left forearm revealed non-caseating granulomas without lymphocyte infiltration. There were no indications of infection by *Mycobacterium*.

The clinical symptoms and pathological findings on the biopsied skin indicated that the patient suffered from EOS. It has been reported that EOS and BS have a common genetic aetiology due to mutations in the *NOD2* gene that cause constitutive Nuclear Factor (NF)-κB activation [4, 5]. Thus we analysed the *NOD2* gene from the patient to look for mutations that might correlate with the pathology of EOS. A written informed consent was obtained from the patient and his families, according to the protocol of the institutional review board of Kyoto University Hospital and in accordance with the Declaration of Helsinki. Genomic sequencing analysis of the patient's *NOD2* gene showed the presence of a heterozygous deletion of six bases in exon 4, which resulted in c.1493_1498delAACTGT, p.E498V, 499–500del (Fig. 1A). The mutation was novel and was not identified in 100 normal controls. A genome alignment of *NOD2* among several species showed that E498, L499 and L500 are conserved from zebrafish to human (Fig. 1B). These data strongly suggested that the identified deletion of six bases in the *NOD2* gene is not a single nucleotide polymorphism (SNP), but is probably responsible for EOS in the patient.

Previous studies report that *NOD2* mutations causing EOS/BS show constitutive activation of NF-κB [6–8]. Therefore, we investigated the level of NF-κB activity associated with the new mutation identified here. First, we confirmed the level of mRNA expression of the mutated allele by subcloning analysis of *NOD2*-cDNA, which showed that the mutated allele was expressed as well as the wild type allele (data not shown). We then evaluated the ability of the *NOD2* mutant to constitutively activate NF-κB by using an *in vitro* reporter system in HEK293T cells transfected with both *NOD2* mutants and NF-κB reporter plasmids (Fig. 1C). The deletion mutant demonstrated almost five times more NF-κB activity than wild type without muramyl dipeptide (MDP) stimulation. Western blot analysis confirmed that NOD2 mutant protein expression was similar to that of wild type (Fig. 1C). Thus, like other mutations of *NOD2* identified previously, the deletion mutant identified here also showed constitutive activation of NF-κB.

The mechanism underlying EOS/BS has not been totally understood, although two pathways downstream from *NOD2* have been identified: NF-κB activation through receptor-interacting protein (RIP) like interacting caspase-like apoptosis regulatory protein kinase (RICK) and MAP kinase activation through the caspase recruitment domain 9 (CARD9) [9]. We previously tested 10 *NOD2* missense mutations that have been identified in our cohort of EOS/BS patients in Japan, and all of them demonstrated constitutive activation of NF-κB [3]. By analysing this newly identified deletion mutant, we have further confirmed the importance of constitutive activation of NF-κB by mutated *NOD2* for the pathogenesis of EOS/BS. We would like to emphasize the

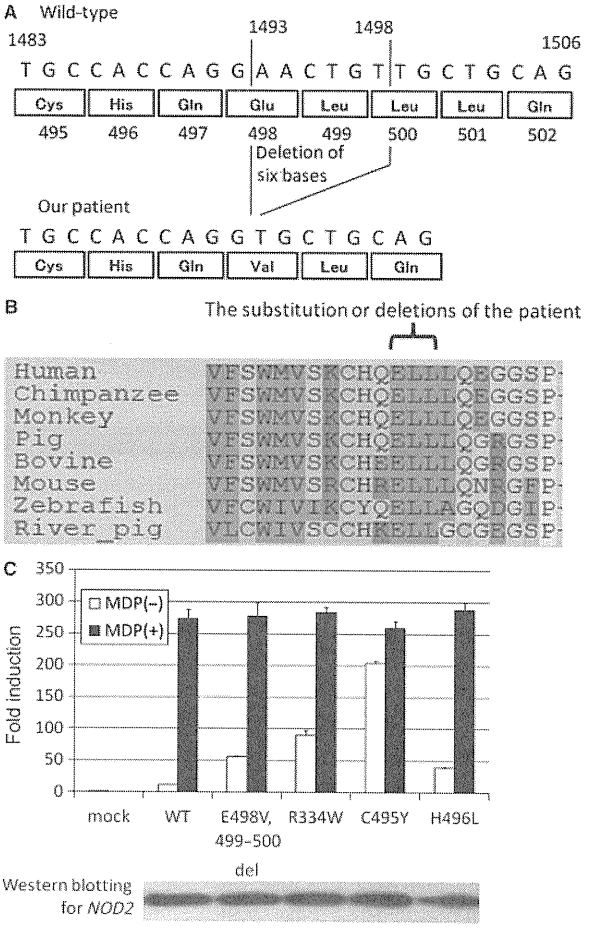

FIG. 1 (**A**) Summary of the mutations identified in our patient. (**B**) NOD2 protein alignment among different species on the mutated amino acids. (**C**) NF-κB reporter assay using the *NOD2* deletion mutant. *In vitro* NF-κB reporter assays were performed as previously described [1, 3, 6, 7]. Mock vector, wild type *NOD2* (WT) and three *NOD2* variants (R334W, C495Y, H496L) derived from EOS/BS patients, were used as controls. Values represent the mean of normalized data (mock without MDP = 1) of triplicate cultures, and error bars indicate S.D. Shown is one representative result of three independent experiments. Protein expression levels of *NOD2* mutants analysed by western blotting are shown in the bottom panel.

usefulness of the NF-κB reporter assay with mutant *NOD2* for observing its role in EOS/BS, although the MAP kinase activation pathway and other possible pathways need to be evaluated to more completely understand the pathogenesis of the *NOD2* mutation in EOS/BS.

We have identified the first deletion mutation in the *NOD2* gene responsible for EOS/BS, and the mutant showed constitutive activation of NF-κB, which is one of the key features that lead to the pathogenesis of EOS/BS.

Rheumatology key message

- A six-base deletion in *NOD2* gene causes EOS.

Acknowledgement

This work was carried out at Department of Pediatrics, Kyoto University Graduate School of Medicine, Kyoto, Japan.

Funding: This work was supported by grants from the Japanese Ministry of Education, Culture, Sports, Science and Technology and grants from the Japanese Ministry of Health, Labor and Welfare.

Disclosure statement: The authors have declared no conflicts of interest.

Hidemasa Sakai[1], Shusaku Ito[2], Ryuta Nishikomori[1], Yuuki Takaoka[1], Tomoki Kawai[1], Megumu Saito[1], Ikuo Okafuji[3], Takahiro Yasumi[1], Toshio Heike[1] and Tatsutoshi Nakahata[1]

[1]*Department of Pediatrics, Kyoto University Graduate School of Medicine, Kyoto,* [2]*Department of Dermatology, Hitachi General Hospital, Hitachi and* [3]*Department of Pediatrics, Kobe City Medical Center General Hospital, Kobe, Japan*
Accepted 27 August 2009
Correspondence to: Ryuta Nishikomori, Department of Pediatrics, Kyoto University Graduate School of Medicine, 54 Kawahara-cho, Shogoin, Sakyo-ku, Kyoto 606-8507, Japan. E-mail: rnishiko@kuhp.kyoto-u.ac.jp

References

1 Rosé CD, Wouters CH, Meiorin S *et al*. Pediatric granulomatous arthritis: an international registry. Arthritis Rheum 2006;54:3337–44.

2 Aróstegui JI, Arnal C, Merino R *et al*. *NOD2* gene-associated pediatric granulomatous arthritis: clinical diversity, novel and recurrent mutations, and evidence of clinical improvement with interleukin-1 blockade in a Spanish cohort. Arthritis Rheum 2007;56:3805–13.

3 Okafuji I, Nishikomori R, Kanazawa N *et al*. Role of the *NOD2* genotype in the clinical phenotype of Blau syndrome and Early-onset sarcoidosis. Arthritis Rheum 2009;60:242–50.

4 Kanazawa N, Okafuji I, Kambe N *et al*. Early-onset sarcoidosis and *CARD15* mutations with constitutive nuclear factor κB activation: common genetic etiology with Blau syndrome. Blood 2005;105:1195–97.

5 Rosé CD, Doyle TM, McIlvain-Simpson G *et al*. Blau syndrome mutation of *CARD15/NOD2* in sporadic early onset granulomatous arthritis. J Rheumatol 2005;32:373–5.

6 Chamaillard M, Philpott D, Girardin SE *et al*. Gene-environment interaction modulated by allelic heterogeneity in inflammatory diseases. Proc Natl Acad Sci USA 2003;100:3455–60.

7 Becker ML, Rosé CD. Blau syndrome and related genetic disorders causing childhood arthritis. Curr Rheumatol Rep 2005;7:427–33.

8 Kambe N, Nishikomori R, Kanazawa N. The cytosolic pattern-recognition receptor NOD2 and inflammatory granulomatous disorders. J Dermatol Sci 2005;39:71–80.

9 Hsu YM, Zhang Y, You Y *et al*. The adaptor protein CARD9 is required for innate immune responses to intracellular pathogens. Nat Immunol 2007;8:198–205.

Rheumatology 2010;49:196–197
doi:10.1093/rheumatology/kep330
Advance Access publication 25 October 2009

Comment on: Hepatotoxicity rates do not differ in patients with rheumatoid arthritis and psoriasis treated with methotrexate

Sir, We read with interest the recent article by Amital *et al*. [1] that compared hepatotoxicity rates in PsA and RA patients treated with MTX based on the evaluation of standard liver function tests. The authors conclude that the incidence of hepatotoxicity does not differ between the two disease groups after adjusting for the cumulative dose of MTX.

Several studies in MTX-treated psoriasis patients have reported that isolated abnormalities of liver enzymes (i.e. alkaline phosphatase, aspartate aminotransferase and alanine aminotransferase) were poor predictors of the severity of liver histopathology. The authors state that the combined sensitivity of aspartate aminotransferase, alanine aminotransferase and bilirubin for detecting an abnormal liver biopsy has been rated at 0.86 based on a previous study [2]. This figure implies that 14% of those with normal liver function tests will have undetected hepatic disease. Larger studies have suggested that 30–50% of the psoriasis patients on MTX have normal standard liver function test results despite histology showing fibrosis and cirrhosis [3]. The lack of correlation between liver enzymes and hepatic fibrosis and cirrhosis has been the major factor leading to the recommendation that liver biopsies be done to monitor potential hepatotoxicity. In this study, the liver function tests were performed with varying frequency which could allow abnormal liver function tests to be missed. The authors acknowledge that the rates of other hepatotoxic agents such as alcohol use and the occurrence of other hepatic comorbidities were not known. We believe that these are significant confounding variables, which make the interpretation of the results of this study difficult. The British Association of Dermatologists recommends serial monitoring

The FASEB Journal • Research Communication

Generation of skeletal muscle stem/progenitor cells from murine induced pluripotent stem cells

Yuta Mizuno,[*,1] Hsi Chang,[*,1] Katsutsugu Umeda,[*] Akira Niwa,[*] Toru Iwasa,[*] Tomonari Awaya,[*] So-ichiro Fukada,[§] Hiroshi Yamamoto,[§] Shinya Yamanaka,[†,‡,‖] Tatsutoshi Nakahata,[*,‡] and Toshio Heike[*,2]

[*]Department of Pediatrics, Graduate School of Medicine, [†]Department of Stem Cell Biology, Institute for Frontier Medical Sciences, and [‡]Center for iPS Cell Research and Application, Institute for Integrated Cell-Material Sciences (iCeMS), Kyoto University, Kyoto, Japan; [§]Department of Immunology, Graduate School of Pharmaceutical Sciences, Osaka University, Osaka, Japan; and [‖]CREST, Japan Science and Technology Agency, Kawaguchi, Japan

ABSTRACT **Induced pluripotent stem (iPS) cells, which are a type of pluripotent stem cell generated from reprogrammed somatic cells, are expected to have potential for patient-oriented disease investigation, drug screening, toxicity tests, and transplantation therapies. Here, we demonstrated that murine iPS cells have the potential to develop *in vitro* into skeletal muscle stem/progenitor cells, which are almost equivalent to murine embryonic stem cells. Cells with strong *in vitro* myogenic potential effectively were enriched by fluorescence-activated cell sorting using the anti-satellite cell antibody SM/C-2.6. Furthermore, on transplantation into *mdx* mice, SM/C-2.6$^+$ cells exerted sustained myogenic lineage differentiation in injured muscles, while providing long-lived muscle stem cell support. Our data suggest that iPS cells have the potential to be used in clinical treatment of muscular dystrophies.—Mizuno, Y., Chang, H., Umeda, K., Niwa, A., Iwasa, T., Awaya, T., Fukada, S., Yamamoto, H., Yamanaka, S., Nakahata, T., Heike, T. Generation of skeletal muscle stem/progenitor cells from murine induced pluripotent stem cells. *FASEB J.* 24, 2245–2253 (2010). www.fasebj.org**

Key Words: Duchenne muscular dystrophy · Pax7 · long-term engraftment · no teratoma formation · high engraftment efficiency

TO MAINTAIN HOMEOSTASIS, SKELETAL muscle fibers are continuously regenerated by activated satellite cells (1), the muscle-specific stem cells that differentiate into myoblasts and form myotubes to replace the myofibers damaged by exercise and daily activities (2). The muscular dystrophies are inherited myogenic disorders of variable distribution and severity that are characterized by progressive muscle wasting and weakness (3). In many forms of muscular dystrophy, the common molecular defect of the encoded proteins, which are involved in muscular structural integrity, is observed in both immature satellite cells and mature myofibers (4). Duchenne muscular dystrophy (DMD), which is the best-described and most serious form of muscular dystrophy, results from mutations in the X-linked dystrophin gene (5). Dystrophin and its associated proteins are commonly known to be indispensable for the functioning of the intracellular actin cytoskeleton, as are laminins in the extracellular matrix of muscle fibers, which protect myofibers from contraction-induced damage (6). Loss of dystrophin causes the rapid and continuous damage of muscles, which leads to the exhaustion of both skeletal muscles and satellite cells, even though muscular regeneration occurs at a higher frequency in DMD patients than in nonaffected individuals (7). Despite extensive efforts to establish pharmacological agents that halt the clinical course of DMD, the disease still results in high mortality in patients during late adolescence.

Skeletal muscle stem/progenitor cell transplantation is considered to be one of the most promising therapies for the muscular dystrophies. In fact, a recent report has shown that the transplanted satellite cells can engraft as myofibers with normal dystrophin expression in the muscles of *mdx* mice, a mouse model of DMD (8, 9). Most of the clinical trials involving allogeneic transplantation of DMD, however, have not obtained satisfactory results due to immune rejection, rapid death, and limited migration of transplanted myoblasts (10).

Embryonic stem (ES) cells have considerable advantages over somatic stem cells as a cell source of transplantation due to their capacity for unlimited proliferation in an undifferentiated state over a prolonged period, and their ability to differentiate into various lineages of cells in the same way as observed *in vivo* (11). Recently, mouse and human induced pluripotent stem (iPS) cells have been established by introducing 3 or 4 pluripotency-associated genes into somatic cells (12–21). Like ES cells, these reprogrammed somatic cells possess properties of self-renewal and pluripotency, and yield germline adult chimeras. Furthermore, the iPS cell technology enables us to generate individualized stem cells, which is expected to contribute to patient-oriented disease studies, drug screenings, toxicity tests, and transplantation therapies (22, 23).

[1] These authors contributed equally to this work.

[2] Correspondence: Department of Pediatrics, Graduate School of Medicine, Kyoto University 54 Kawahara-cho, Shogoin, Sakyo-ku Kyoto 606-8507, Japan. E-mail: heike@kuhp.kyoto-u.ac.jp

doi: 10.1096/fj.09-137174

We demonstrated previously that long-lived muscle stem cells can successfully be induced from murine ES (mES) cells *in vitro* by plating embryoid bodies (EBs) onto Matrigel-coated plates (24). These ES cell-derived $Pax7^+$ cells can be enriched effectively by the SM/C-2.6 antibody, an anti-satellite cell antibody (25), and possess a potential to differentiate into myofibers both *in vitro* and *in vivo*. Here, we demonstrated that by using our induction system, SM/C-2.6^+ myogenic lineages were induced successfully from murine iPS (miPS) cells. This system enabled quantitative assays of mature and immature skeletal muscular lineage cells both *in vitro* and *in vivo* and may serve as a useful experimental tool for the treatment of various muscular dystrophies.

MATERIALS AND METHODS

Cell lines

A 4-factor miPS cell line reprogrammed by the introduction of *Oct3/4*, *Sox2*, *Klf4*, and *c-Myc* (clone 38D2), and a 3-factor iPS cell line that lacks *c-Myc* (clone 256H-18), were established from murine embryonic fibroblasts. These fibroblasts carried the Nanog-GFP-IRES-$Puro^r$ reporter and the tail-tip fibroblasts of adult *Discosoma* sp. red fluorescent protein (DsRed)-transgenic mice, respectively, and were maintained as described previously (13, 14). The enhanced green fluorescent protein (GFP)-transfected ES cell line D3, a kind gift from Dr. Masaru Okabe (Osaka University, Osaka, Japan), was maintained as reported elsewhere (24, 26).

In vitro differentiation of ES cells and iPS cells into a muscle cell lineage

Differentiation of mES and miPS cells was based on a previously established protocol (24). Briefly, in order to eliminate feeder cells, undifferentiated mES and miPS cells were treated with 0.5% trypsin/ethylenediaminetetraacetic acid (Life Technologies, Inc., Grand Island, NY, USA; http://www.invitrogen.com) and transferred onto tissue culture dishes (Falcon; BD Biosciences, San Diego, CA, USA; http://www.bdbiosciences.com) coated with 0.1% gelatin (Sigma-Aldrich, St. Louis, MO, USA; http://www.sigmaaldrich.com) in maintenance medium supplemented with 5000 U/ml leukemia inhibitory factor (LIF), at a concentration of 5×10^3 cells/cm^2. For embryoid body (EB) formation, mES and miPS cells were cultured in hanging drops for 3 d at a density of 800 cells/20 μl differentiation medium, consisting of Dulbecco's modified Eagle medium (DMEM) supplemented with 10% fetal calf serum (FCS), 5% horse serum (Sigma), 0.1 mM 2-mercaptoethanol, 0.1 mM nonessential amino acid, and 50 μg/ml penicillin/streptomycin. EBs were then transferred to a suspension culture in the differentiation medium for an additional 3 d. Finally, each EB was plated onto 48-well tissue culture plates (Falcon) coated with Matrigel Basement Membrane Matrix (BD Bioscience, Bedford, MA, USA; http://www.bdbiosciences.com). The medium was changed every 5 d.

Immunostaining

Immunofluorescence and immunocytochemical analyses were performed as described previously (24). Primary antibodies (Abs) used in this study included mouse anti-Pax3, mouse anti-Pax7 (R&D Systems, Minneapolis, MN, USA; http://www.rndsystems.com), rabbit anti-Myf5 (Santa Cruz Biotechnology, Inc., Santa Cruz, CA, USA; http://www.scbt.com), mouse anti-MyoD1, mouse anti-myogenin (Dako, Carpinteria, CA, USA; http://www.dako.com), mouse anti-myosin heavy chain (MHC) (Zymed Laboratories, San Francisco, CA, USA; http://www.invitrogen.com), rabbit anti-DsRed (Clontech Laboratories Inc., Palo Alto, CA, USA; http://www.clontech.com), rat anti-laminin-α2 (4H8–2; Alexis Biochemicals, San Diego, CA, USA; http://www.axxora.com), and mouse anti-dystrophin (MANDRA1; Sigma). The secondary Abs used in this study were Cy3-conjugated anti-mouse, anti-rabbit, or anti-rat IgG (Jackson ImmunoResearch Laboratories Inc., West Grove, PA, USA; http://www.jacksonimmuno.com), fluorescein isothiocyanate (FITC)-conjugated anti-mouse or anti-rat IgG (Jackson ImmunoResearch), and Alexa 633-conjugated anti-rat IgG (Molecular Probes, Eugene, OR, USA; http//probes.invitrogen.com). Vectastain ABC Kit and DAB substrate Kit (Vector Laboratories, Burlingame, CA, USA; http://www.vectorlabs.com) was used for diaminobenzidine (DAB) staining. Hoechst 33342 (Molecular Probes) was used for nuclear staining. For the *in vivo* myogenic differentiation assay, the engrafted muscles were isolated and frozen in liquid nitrogen-cooled isopentane (25). The Vector® M.O.M.™ Immunodetection Kit (Vector Laboratories) was used to prevent nonspecific secondary antibody from binding to Fc receptors in the frozen sections. The samples were then examined using a fluorescent microscope (FluoView System; Olympus, Tokyo, Japan; http://www.olympus-global.com) or an AS-MDW system (Leica Microsystems GmbH, Wetzlar, Germany; http://www.leica.com). Photographs were acquired with an AxioCam (Carl Zeiss Vision GmbH, Hallbergmoos, Germany; http://www.zeiss.com) or an AS-MDW system (Leica Microsystems GmbH). DAB and HE staining were performed as previously reported (27).

RT–PCR analysis

RNA isolation and RT–PCR were performed according to previously established protocols (24). The oligonucleotide primers for *Pax3*, *Pax7*, *Myf5*, *MyoD*, *Myogenin*, and *GAPDH* were described elsewhere (24).

Flow-cytometric (FCM) analysis and cell sorting

Staining procedures, FCM analysis, and cell sorting were performed as described previously (24). On d 20, EBs were collected and treated with enzyme-free Hank's-based Cell Dissociation Buffer (Invitrogen, Carlsbad, CA, USA; http://invitrogen.com) for 30 min at 37°C, and gently dissociated into single cells. The resultant cells were stained with biotin-conjugated or rat SM/C-2.6 antibody (25) and then with allophycocyanin (APC)-conjugated streptavidin or anti-rat IgG (Becton Dickinson Labware, San Jose, CA, USA; http://www.bd.com). The primary Abs used for FCM analysis included mouse anti-CD34 (Becton Dickinson), mouse anti-CD56 (Biolegend, San Diego, CA, USA; http://www.biolegend.com), mouse anti-M-cadherin (Calbiochem, San Diego, CA, USA; http://www.calbiochem.com), mouse anti-c-Met, and mouse anti-integrin α7 (R&D Systems). The secondary Abs used in this study were PE- or FITC-conjugated anti-mouse IgG (Becton Dickinson). Dead cells were excluded by propidium iodide (PI) (Sigma) or 4′,6-diamidino-2-phenylindole (DAPI; Sigma) staining. Samples were analyzed using a FACSCalibur apparatus and the Cell Quest software (Becton Dickinson). Cell sorting with the SM/C-2.6 Ab was performed using a FACSVantage flow cytometer (Becton Dickinson).

Intramuscular cell transplantation

Male *mdx* mice (Central Laboratories for Experimental Animals, Kanagawa, Japan; http://www.clea-Japan.com), aged 6–8 wk, which originated from the C57BL/10 strain, were used as

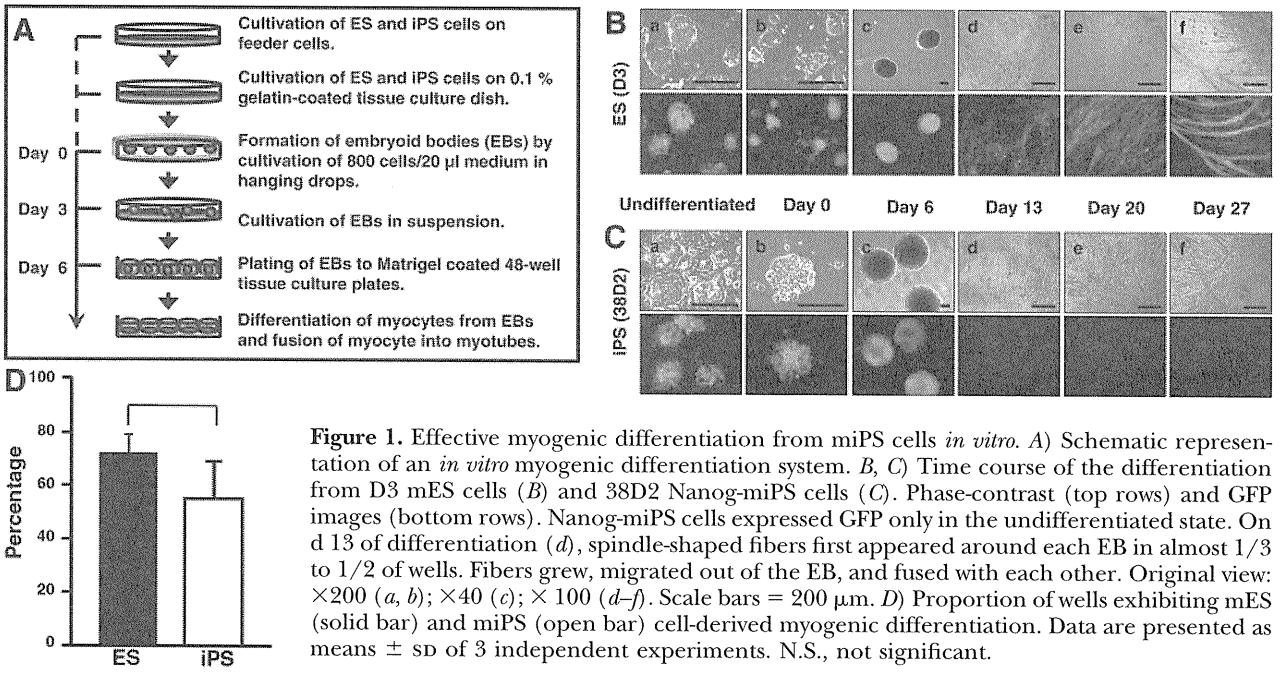

Figure 1. Effective myogenic differentiation from miPS cells *in vitro*. *A*) Schematic representation of an *in vitro* myogenic differentiation system. *B, C*) Time course of the differentiation from D3 mES cells (*B*) and 38D2 Nanog-miPS cells (*C*). Phase-contrast (top rows) and GFP images (bottom rows). Nanog-miPS cells expressed GFP only in the undifferentiated state. On d 13 of differentiation (*d*), spindle-shaped fibers first appeared around each EB in almost 1/3 to 1/2 of wells. Fibers grew, migrated out of the EB, and fused with each other. Original view: ×200 (*a, b*); ×40 (*c*); × 100 (*d–f*). Scale bars = 200 µm. *D*) Proportion of wells exhibiting mES (solid bar) and miPS (open bar) cell-derived myogenic differentiation. Data are presented as means ± SD of 3 independent experiments. N.S., not significant.

recipient mice throughout the experiment. The miPS cell line (clone 256H-18), which arose from B6, was used as the source of donor cells. In the major histocompatibility complex, the H2 haplotypes of *mdx* mice and iPS cells are both of type *b*.

Intramuscular cell transplantation was performed according to an earlier experiment (24). Briefly, the recipient *mdx* mice (28) were injured with 50 µl of 10 µM cardiotoxin (CTX; Latoxan, Valence, France; http://www.latoxan.com) in the left

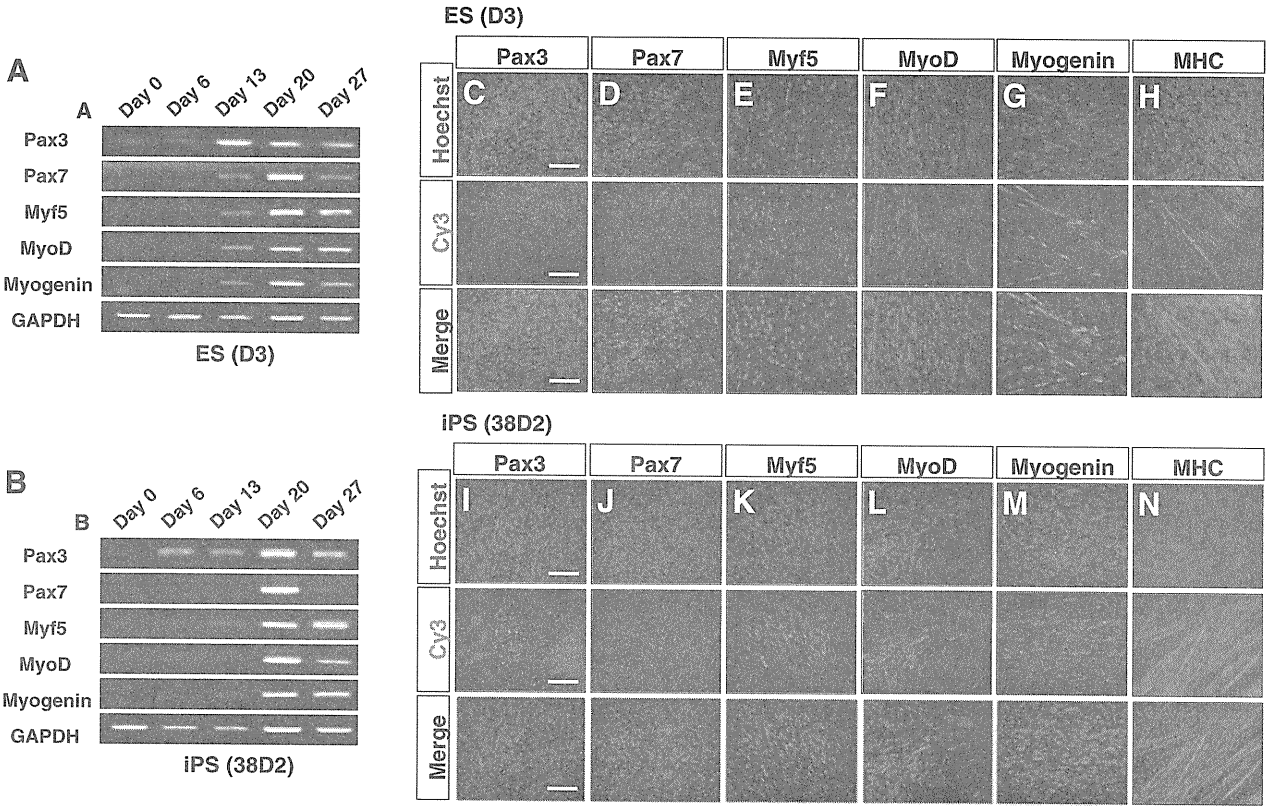

Figure 2. Myogenic marker analysis in mES and miPS cell-derived cultures. *A, B*) Sequential RT–PCR analysis of skeletal myogenesis-related genes. Data for D3 mES cells (*A*) and 38D2 miPS cells (*B*). For semiquantitative comparison, samples were normalized by dilution to produce equivalent signals for *GAPDH*. *C–N*) Skeletal myofibers were observed in cultures, which were positive for anti-Pax3 (*C, I*), anti-Pax7 (*D, J*), anti-Myf5 (*E, K*), anti-MyoD (*F, L*), anti-myogenin (*G, M*), and anti-MHC (*H, N*) Abs on d 20 of differentiation. Data for D3 mES cells (*C–H*) and 38D2 miPS cells (*I–M*). mES and miPS cell-derived cultures were analyzed using Cy3. Nuclei were costained with Hoechst 33342 (blue). Original view: ×200. Scale bars = 100 µm.

tibialis anterior (LTA) muscle 24 h before transplantation (29, 30). The mice then received 6 Gy of systematic irradiation 12 h before transplantation (modified from refs. 31, 32). The sorted 3×10^4 cells from each fraction were resuspended in 20 μl of differentiation medium. The same batch of sorted cells was then injected into the LTA muscle of the recipient *mdx* mice with an Allergy Syringe (Becton Dickinson). At 4 and 24 wk after transplantation, we counted the number of engrafted DsRed$^+$ skeletal myofibers that were immunopositive for the anti-laminin Ab per field at ×200, with a mean value of 3 sections/tissue sample. Engraftment efficiency was defined as the percentage of DsRed$^+$ fibers per total number of injected cells. All animal-handling procedures followed the Guide for the Care and Use of Laboratory Animals published by the U.S. National Institutes of Health (NIH Publication No. 85–23, revised 1996) and the Guidelines of the Animal Research Committee of the Graduate School of Medicine, Kyoto University.

Statistics

Data are shown as averages ± SD. Statistical analyses were conducted using the unpaired Student's *t* test, and significance was set at $P < 0.05$, $P < 0.01$, or $P < 0.001$.

RESULTS

Efficient skeletal muscle differentiation from miPS cells *in vitro*

We initiated the differentiation of skeletal muscle fibers from miPS cells *in vitro* using a protocol previously established for mES cells (**Fig. 1***A*) (24). In this culture system, both mES and miPS cells formed EBs after the initial 6 d in a hanging drop and suspension culture. The EBs quickly attached to the plates and, 7 d after plating onto the Matrigel-coated plates (d 13 of differentiation), spindle-shaped fibers appeared around the EBs in almost 1/3 to 1/2 of wells. After 14 d of plating (d 20 of differentiation), these spindle fibers grew, migrated out of the EB, and began to fuse with each other, forming thick multinucleated fibers resembling normal skeletal myofibers (Fig. 1*B*, *C*). In 38D2 miPS cell-derived cultures, GFP expression was not observed from d 13 of differentiation, indicating that the undifferentiated

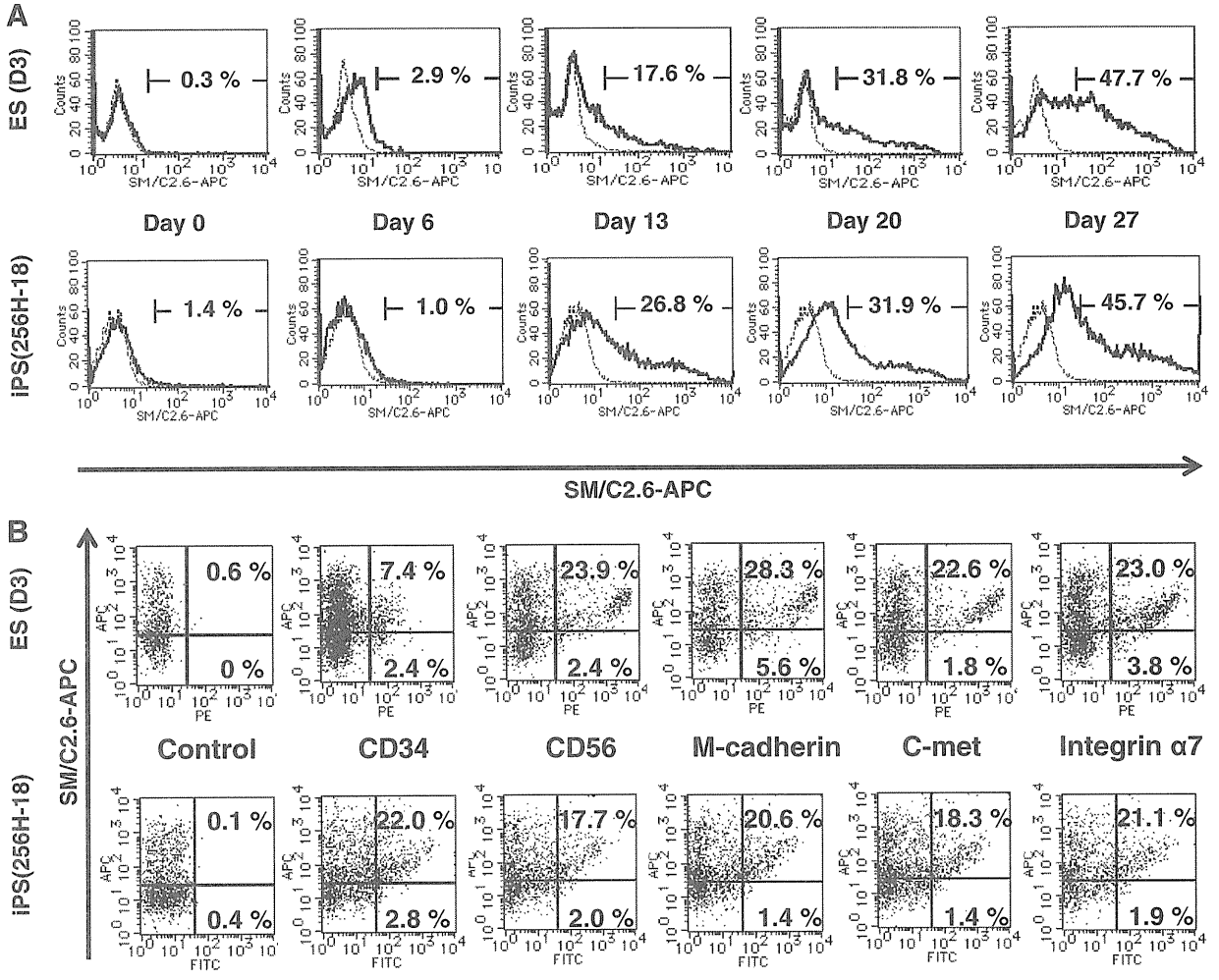

Figure 3. Development of SM/C-2.6$^+$ cells from miPS cells during myogenic differentiation. *A*) Sequential FACS analysis of SM/C-2.6 during induction of differentiation. Cultures were analyzed on d 0, 6, 13, 20, and 27. Data for D3 mES cells (top row) and 256H-18 miPS cells (bottom row). Percentage of SM/C-2.6$^+$ cells among total live GFP$^+$ or DsRed$^+$ cells is indicated. Plots show isotypic control staining profiles (dashed lines) *vs.* the anti-SM/C-2.6 Ab staining profiles (solid lines). *B*) FACS analysis of myogenic stem/progenitor cell-related surface markers. Data for D3 mES cells (top row) and 256H-18 miPS cells (bottom row). Percentages represent fraction of cells expressing a given surface antigen among total live GFP$^+$ or DsRed$^+$ cells. Representative results from 1 of 3 independent experiments are shown.

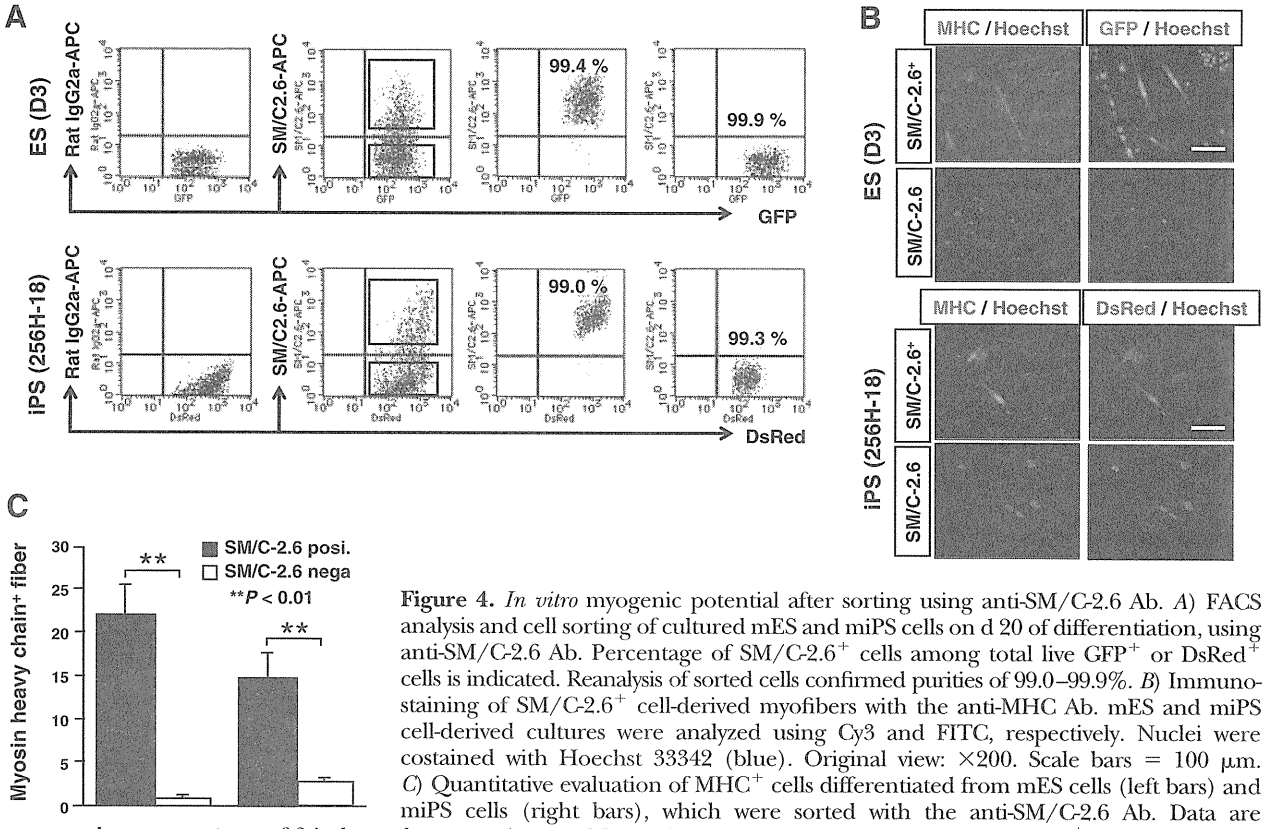

Figure 4. *In vitro* myogenic potential after sorting using anti-SM/C-2.6 Ab. *A*) FACS analysis and cell sorting of cultured mES and miPS cells on d 20 of differentiation, using anti-SM/C-2.6 Ab. Percentage of SM/C-2.6$^+$ cells among total live GFP$^+$ or DsRed$^+$ cells is indicated. Reanalysis of sorted cells confirmed purities of 99.0–99.9%. *B*) Immunostaining of SM/C-2.6$^+$ cell-derived myofibers with the anti-MHC Ab. mES and miPS cell-derived cultures were analyzed using Cy3 and FITC, respectively. Nuclei were costained with Hoechst 33342 (blue). Original view: ×200. Scale bars = 100 μm. *C*) Quantitative evaluation of MHC$^+$ cells differentiated from mES cells (left bars) and miPS cells (right bars), which were sorted with the anti-SM/C-2.6 Ab. Data are presented as means ± SD of 3 independent experiments. Myogenic activity was restricted to the SM/C-2.6$^+$ cell fraction.

marker Nanog had been inactivated during differentiation. We also observed the spontaneous contraction of the fibers on d 27 of differentiation, just as seen in normal skeletal myofibers (Supplemental Video S1).

We then used RT–PCR to examine the expression of genes associated with skeletal myogenesis (**Fig. 2***A, B*). Pax3 and Pax7, which are expressed selectively by satellite cells, are essential for the specifying myogenic progenitors from the central dermomyotome (33). Subsequently, the stem/progenitor cells display myogenic properties by expressing muscle regulatory factors (MRFs), such as Myf5, MyoD, and myogenin (2, 34, 35). Among the myogenic progenitor-related genes and MRFs, only Pax3 was expressed at low levels in both mES and miPS cells on d 6. The expression of all myogenic marker genes was apparent from d 13 of differentiation onward, and peaked on d 20 of differentiation in both mES and miPS cell-derived cultures. Immunostaining for Pax3 (Fig. 2*C, I*), Pax7 (Fig. 2*D, J*), Myf5 (Fig. 2*E, K*), MyoD (Fig. 2*F, L*), and myogenin (Fig. 2*G, M*) also confirmed the development of skeletal muscular lineage cells on d 20 of differentiation. Fibers were positive for MHC, a specific marker of mature myofibers (Fig. 2*H, N*). The proportion of wells containing myofibers was 71.9 ± 6.9% for mES cells and 54.9 ± 13.9% for miPS cells (P=0.065) (Fig. 1*D*). A similar myogenic development was also observed for clone 256H-18, an miPS cell line generated from three factors, without *c-Myc* (Supplemental Fig. S1). Collectively, these results demonstrated that, like mES cells, miPS cells had a high potential to differentiate into myogenic lineages *in vitro*.

Development of miPS-derived SM/C-2.6$^+$ cells during myogenic differentiation

Isolating of living stem/progenitor cells is desirable for clinical applications of *in vitro* pluripotent stem cell cultures (30, 36, 37). We therefore investigated the

TABLE 1. *Summary of intramuscular cell transplantation*

Group	Mouse	DsRed+ fibers/TA	Engraftment efficiency (%)
SM/C-2.6$^+$ (4W)	1	73	0.2
	2	120	0.4
	3	20	0.1
	4	74	0.3
	5	44	0.2
	6	19	0.1
	Mean	58.3 ± 38.7	0.2 ± 0.1
SM/C-2.6$^-$ (4W)	1	10	
	2	8	0
	3	0	0
	Mean	3 ± 4.4	0 ± 0
SM/C-2.6$^+$ (24W)	1	249	0.8
	2	313	1
	3	212	0.7
	Mean	258 ± 51.1	0.8 ± 0.2

Sorted SM/C-2.6$^+$ or SM/C-2.6$^-$ cells (3×10^4) were injected into the preinjured left tibialis (TA) muscle of *mdx* mice. Four (4W) and 24 wk (24W) after transplantation, numbers of DsRed$^+$ myofibers per field in the injured TA were counted at ×200 with a mean value of 3 sections/tissue sample. Engraftment efficiency was defined as the percentage of DsRed$^+$ fibers per total number of injected cells.

expression of SM/C-2.6, an effective antisatellite/satellite-like cell surface marker for murine skeletal muscle and mES cells (25). Sequential FACS analyses showed that SM/C-2.6$^+$ cells were detected on d 13 and increased during further differentiation of mES and miPS cells (**Fig. 3***A*). Thus, the kinetics of SM/C-2.6 expression correlated with the development of myofibers and with the up-regulation of the expression of skeletal myogenesis-related genes.

We then examined the expression of CD34, CD56, M-cadherin, c-Met, and Integrin α7, which are surface markers expressed by satellite cells (2). About 20% of miPS cell-derived SM/C-2.6$^+$ cells expressed CD34, CD56, M-cadherin, c-Met, and integrin α7, whereas expression of these surface markers was hardly detected in the SM/C-2.6$^-$ cell fraction (Fig. 3*B*). All of the given surface markers had similar expression patterns in both mES and miPS cell-derived SM/C-2.6$^+$ cells. Thus, the characterization of miPS cell-derived SM/C-2.6$^+$ cells revealed that these cells contained the surface antigens expressed by satellite cells.

Myogenic potential of miPS cell-derived SM/C-2.6$^+$ cells *in vitro*

Given the results described above, we attempted to analyze the capacity of miPS cell-derived SM/C-2.6$^+$ cells to generate myogenic lineages *in vitro* and *in vivo*. We collected all the cultured mES and miPS cells from the tissue culture plates on d 20 of differentiation and sorted them with the SM/C-2.6 Ab (**Fig. 4***A*). To assess myogenic differentiation *in vitro*, the sorted 5×10^3 cells were replated onto new Matrigel-coated 96-well plates on d 20, and the myofibers generated were assayed by immunostaining with the anti-MHC Ab 7 d after replating. Myogenic activity was detected in the SM/C-2.6$^+$ population from both mES and miPS cell-derived cultures (Fig. 4*B*). The number of myofibers

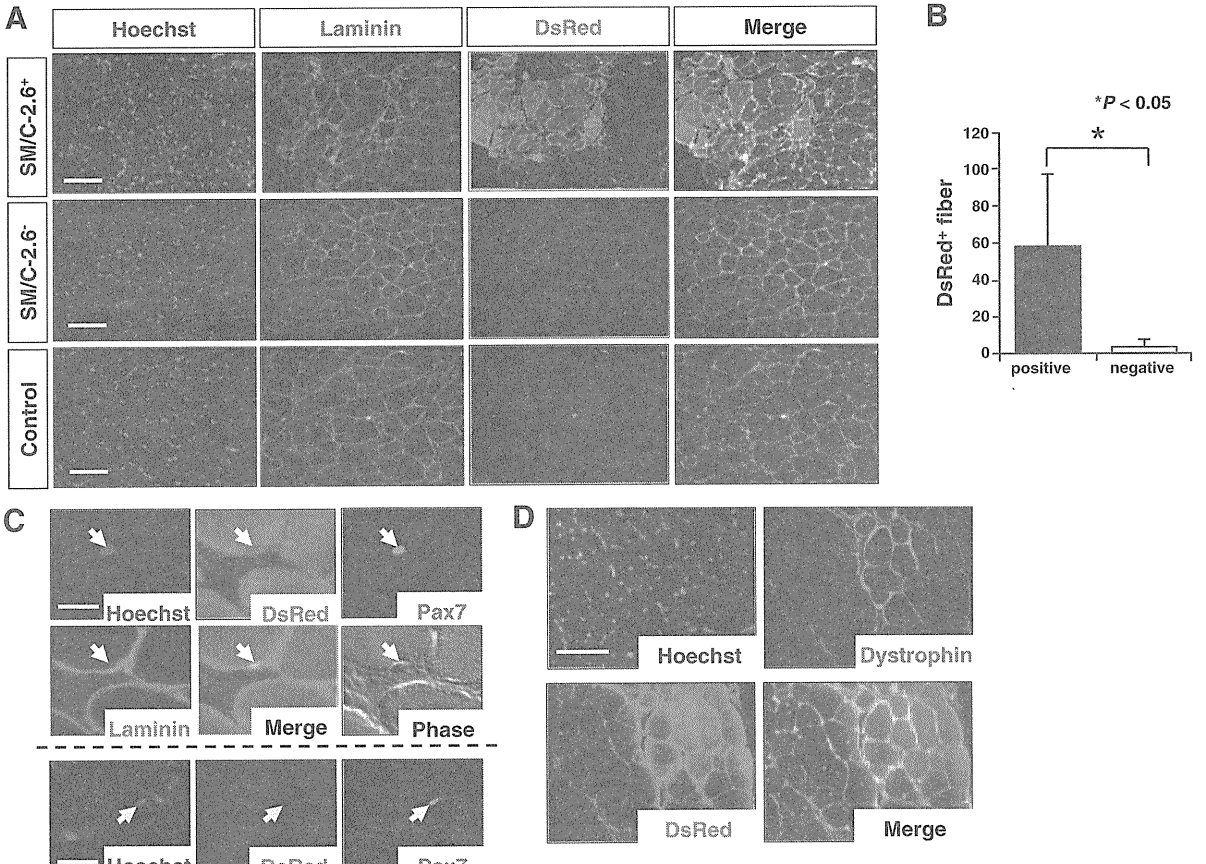

Figure 5. Engraftment of miPS cell-derived SM/C-2.6$^+$ cells into *mdx* mice. *A*) Immunostaining of cells grafted with cultured miPS cells sorted with anti-SM/C-2.6 Ab. Cells were stained with anti-laminin (green) and anti-DsRed (red) Abs. Nuclei were costained with Hoechst 33342 (blue). *B*) Quantitative evaluation of engrafted DsRed$^+$ myofibers from miPS cell-derived SM/C-2.6$^+$ (solid bar) and SM/C-2.6$^-$ (open bar) cells. Data are presented as means ± SD of 6 (SM/C-2.6$^+$ group) or 3 independent samples (SM/C-2.6$^-$ group). *C*) Cells located on DsRed$^+$ (top row) and DsRed$^-$ (bottom row) muscular membrane were stained with anti-DsRed (red) and anti-Pax7 (green) Abs. Nuclei were costained with Hoechst 33342 (blue). White arrows indicate DsRed$^+$/Pax7$^+$ cells; yellow arrows indicate DsRed$^-$/Pax7$^+$ cells. *D*) Cells from recipient *mdx* mice transplanted with SM/C-2.6$^+$ cells were stained with anti-DsRed (red) and anti-dystrophin (green) Abs. Dystrophin protein expression was observed mainly in DsRed$^+$ myofibers, but not in DsRed$^-$ myofibers. Nuclei were costained with Hoechst 33342 (blue). Original view: ×100 (*A*); ×400 (*C*); ×200 (*D*). Scale bars = 100 μm (*A*, *D*); 10 μm (*C*).

per well was 22.0 ± 3.6 and 14.7 ± 3.1 for the mES and miPS cell-derived SM/C-2.6$^+$ populations, respectively (P=0.027) (Fig. 4*C*). Thus, the SM/C-2.6$^+$ cells generated from miPS cells had a potential to differentiate into myogenic lineages *in vitro*, although the efficiency was slightly lower than that of mES cells.

Engraftment of miPS cell-derived SM/C-2.6$^+$ cells into damaged muscles of *mdx* mice

We then investigated the *in vivo* potential of miPS cell-derived SM/C-2.6$^+$ cells by transplanting these cells into *mdx* mice, a well-known model for DMD (28) (**Table 1**). To reduce the possibility of tumor formation after transplantation, we chose to use clone 256H-18, an miPS cell line established without c-Myc transduction (14). The recipient *mdx* mice were injured by CTX and irradiation, and DsRed$^+$ miPS cell-derived SM/C-2.6$^+$ cells were directly injected into the predamaged LTA muscles. Four weeks after transplantation, DsRed$^+$ skeletal myofibers, which were also confirmed by immunostaining with the anti-laminin Ab, were observed exclusively in the muscles transplanted with SM/C-2.6$^+$ cells (**Fig. 5*A***). Successful engraftment was also confirmed by diaminobenzidine (DAB) staining with an anti-DsRed Ab (Supplemental Fig. S2). The number of DsRed$^+$ skeletal myofibers was 58.3 ± 37.8 (n=6) from SM/C-2.6$^+$ cells, and 3.0 ± 4.4 (n=3) from SM/C-2.6$^-$ cells (P=0.024) (Fig. 5*B*). Thus, miPS cell-derived SM/C-2.6$^+$ cells had a greater potential to form muscle fascicles.

We further characterized the fate of the SM/C-2.6$^+$ cells engrafted in the injured muscles. Immunostaining analyses showed that DsRed$^+$/Pax7$^+$ mononuclear cells were located between laminin and the muscular plasma membrane, which is consistent with the location of satellite cells (Fig. 5*C*). In addition, strong dystrophin expression was detected over the entire surface of DsRed$^+$ muscle fascicles, but not in the DsRed$^-$ muscle fascicles (Fig. 5*D*). These results demonstrated that miPS-derived SM/C-2.6$^+$ cells engrafted and differentiated into mature myofibers, and could then restore dystrophin expression *in vivo*, remained as satellite-like cells.

Long-term engraftment of miPS cell-derived skeletal muscle stem/progenitor cells into recipient muscles

Finally, we evaluated the long-term effect of the SM/C-2.6$^+$ cells engrafted in the damaged muscle. In the muscle of *mdx* mice transplanted with SM/C-2.6$^+$ cells, the number of DsRed$^+$ myofibers was significantly higher at 24 wk than that at 4 wk (258.0±51.1; n=3) compared with 58.3 ± 38.7 (n=6; P=0.0001) (**Fig. 6*B***). The presence of mature skeletal muscle fascicles was confirmed by immunostaining with anti-laminin and anti-dystrophin Abs (Fig. 6*A*, *C*). In the engrafted muscle fascicle, most DsRed$^+$ muscles had a typical central nucleus, indicating the presence of freshly regenerated muscle fibers. Furthermore, DsRed$^+$/Pax7$^+$ mononuclear cells were also observed 24 wk after transplantation (data not shown). Teratoma formation was not observed in any of the mice sacrificed 24 wk after transplantation with miPS cells that were sorted using the SM/C-2.6 Ab. In contrast, though no teratoma was formed in mice transplanted with SM/C-2.6$^-$ cells, tissues surrounded by inflammatory cells were observed and were negative for skeletal MHC (Supplemental Fig. S3). Thus, miPS cell-derived skeletal muscle stem/progenitor cells engrafted effectively, promoted differentiation into mature myogenic lineages, and provided long-term stem-cell support to the surrounding muscle tissue without exhaustion.

DISCUSSION

Progressive muscular dystrophies are characterized by the relative exhaustion of satellite cells, whose growth and regeneration cannot compensate for the degeneration of myofibers (7). The effects of the genes/proteins that cause muscular dystrophies may occur as early as the satellite cell stage during muscular regeneration. Thus, muscular dystrophies are thought to be one of the most suitable models for the clinical application of lineage-specific stem cell transplantation.

Several investigations demonstrated the utility of mus-

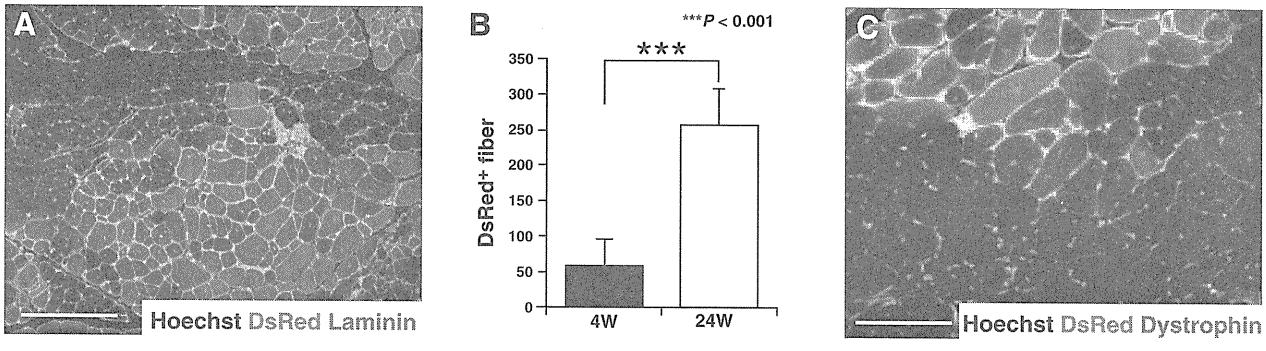

Figure 6. Long-term engraftment of miPS cell-derived skeletal muscle stem/progenitor cells into recipient muscles. *A*) Immunostaining of SM/C-2.6$^+$ cell-derived grafted cells. Mice were analyzed at 24 wk after transplantation. Cells were stained with anti-DsRed (red) and anti-laminin (green) Abs. Nuclei were costained with Hoechst 33342 (blue). *B*) Quantitative evaluation of engrafted DsRed$^+$ myofibers at 4 wk (solid bar) and 24 wk (open bar) after transplantation. Data are presented as means ± SD of 6 (at 4 wk) or 3 independent samples (at 24 wk). Number of DsRed$^+$ myofibers at 24 wk increased when compared with that observed at 4 wk after transplantation. *C*) Cells were stained with anti-DsRed (red) and anti-dystrophin (green) Abs. Nuclei were costained with Hoechst 33342 (blue). Original magnification, ×100. Scale bars = 100 μm.

cle-specific stem/progenitor cells, while myoblast transplantation had limited success in treating muscular dystrophies (38). One of the most critical problems in the clinical trials is the limited number of stem/progenitor cells that can be isolated from the body. Alternative cell sources, such as bone marrow-derived side-population cells (39, 40), mesenchymal stem cells (41), pericytes (42), CD133$^+$ progenitor cells (43), and mesoangioblasts (44), have been shown to have a high myogenic potential *in vitro* and *in vivo*. However, a common disadvantage of approaches that use tissue-specific myogenic stem/progenitor cells is the inability to harvest sufficient quantities of cells.

As for limitless expansion, pluripotent stem cells (ES and iPS cells) are thought to be the most reliable cell source for clinical applications. However, the establishment of individualized pluripotent cells from ES cells is difficult, not only due to technical issues such as production of somatic cell nuclear-transfer ES cells, but also to the ethical restrictions of manipulating human oocytes to obtain the inner cell mass of blastocysts. In contrast, the iPS cell method has a clear advantage in establishing individual pluripotent stem cells, which extends the possibilities of clinical applications. First of all, autologous iPS-derived cell transplantation is expected to rescue patients with various diseases, as a recent study has demonstrated that autologous gene-corrected hematopoietic cells generated from iPS cells can resolve symptoms in sickle-cell anemia model mice (45). Furthermore, the patient-oriented pluripotent stem cells will serve as an experimental tool for developing a clear understanding of the pathophysiology of these diseases, as well as for establishing improved pharmacological models.

iPS cells are artificial pluripotent stem cells that are reprogrammed from somatic cells. Therefore, when considering these cells for use as an experimental tool, it is inevitably required to verify their potential to differentiate into a specific lineage of interest. For this purpose, we addressed the myogenic differentiation potential of miPS cells in a culture system shown previously to efficiently generate satellite-like cells from mES cells (24). Using this modified culture system to plate EBs onto Matrigel-coated dishes, the emergence and proliferation of mature skeletal myofibers was observed in a manner that is almost equivalent to that of mES cells. Sequential RT–PCR analyses revealed that the expression of PAX3 and PAX7 was detected first and was followed by the expression of myogenic markers such as Myf5, MyoD, and Myogenin. These results suggested that a similar profile of myogenic markers is involved during miPS cell differentiation as is observed in normal myogenesis (33, 34).

Our results also confirmed the utility of a recently established anti-satellite cell Ab SM/C-2.6 to enrich for skeletal muscle stem/progenitor cells in the miPS differentiation system, as has been reported in both murine skeletal muscle (25) and in an mES cell culture system (24). The expression of myogenic stem/progenitor cell-related surface markers and myogenic activity was restricted to the SM/C-2.6$^+$ cell fraction both *in vitro* and *in vivo*. Analysis of long-term transplantation over a 24-week period showed a significant increase in the number of miPS-derived DsRed$^+$ muscle fascicles. This result suggests that miPS-derived SM/C-2.6$^+$ cells provided sufficient progeny to repair damaged tissue for an extended period of time. In agreement with our previous report of mES cells (24), we confirmed that selection using the SM/C-2.6 Ab eliminated the possibility of teratoma formation. Collectively, enrichment with the SM/C-2.6 Ab, in combination with an efficient myogenic lineage differentiation culture system, allows quantitative analysis in basic research, as well as mass cultivation for clinical applications.

The miPS cell-derived SM/C-2.6$^+$ cell transplantation yielded encouraging results and may be used to develop a novel strategy for treating muscular dystrophies. In the damaged muscles of *mdx* mice, the sorted stem/progenitor cells engrafted and differentiated successfully into skeletal myofibers surrounded by dystrophin without the formation of pluripotent cell-derived teratomas. Of note, transplanted cells continued to express Pax7 and resided beneath laminin, similar to what is observed in satellite cells during muscle regeneration and in normal skeletal muscle tissues. These observations strongly suggest that a part of the SM/C-2.6$^+$ cells possessed satellite-like properties, which could retain the immature state and may supply stem/progenitor cell support for long-lasting muscle damage in many forms of muscular dystrophies.

In summary, long-lived skeletal muscle stem/progenitor cells were successfully induced from miPS cells using our *in vitro* culture system. In combination with the remarkable technological advances in the creating more practical iPS cell lines, the system presented here will promote further investigations, and give rise to promising clinical trials to combat degenerative muscle disorders. FJ

This work was supported by grants from the Japan Ministry of Education, Culture, Sports, Science, and Technology.

REFERENCES

1. Mauro, A. (1961) Satellite cell of skeletal muscle fibers. *J. Biophys. Biochem. Cytol.* **9,** 493–495
2. Charge, S. B., and Rudnicki, M. A. (2004) Cellular and molecular regulation of muscle regeneration. *Physiol. Rev.* **84,** 209–238
3. Emery, A. E. (2002) The muscular dystrophies. *Lancet* **359,** 687–695
4. Wallace, G. Q., and McNally, E. M. (2008) Mechanisms of muscle degeneration, regeneration, and repair in the muscular dystrophies. *Annu. Rev. Physiol*
5. Hoffman, E. P., Brown, R. H., Jr., and Kunkel, L. M. (1987) Dystrophin: the protein product of the Duchenne muscular dystrophy locus. *Cell* **51,** 919–928
6. Campbell, K. P. (1995) Three muscular dystrophies: loss of cytoskeleton-extracellular matrix linkage. *Cell* **80,** 675–679
7. Jejurikar, S. S., and Kuzon, W. M., Jr. (2003) Satellite cell depletion in degenerative skeletal muscle. *Apoptosis* **8,** 573–578
8. Montarras, D., Morgan, J., Collins, C., Relaix, F., Zaffran, S., Cumano, A., Partridge, T., and Buckingham, M. (2005) Direct isolation of satellite cells for skeletal muscle regeneration. *Science* **309,** 2064–2067
9. Cerletti, M., Jurga, S., Witczak, C. A., Hirshman, M. F., Shadrach, J. L., Goodyear, L. J., and Wagers, A. J. (2008) Highly efficient, functional engraftment of skeletal muscle stem cells in dystrophic muscles. *Cell* **134,** 37–47
10. Partridge, T. A. (1991) Invited review: myoblast transfer: a possible therapy for inherited myopathies? *Muscle Nerve* **14,** 197–212
11. Evans, M. J., and Kaufman, M. H. (1981) Establishment in culture of pluripotential cells from mouse embryos. *Nature* **292,** 154–156

12. Takahashi, K., and Yamanaka, S. (2006) Induction of pluripotent stem cells from mouse embryonic and adult fibroblast cultures by defined factors. *Cell* **126,** 663–676
13. Okita, K., Ichisaka, T., and Yamanaka, S. (2007) Generation of germline-competent induced pluripotent stem cells. *Nature* **448,** 313–317
14. Nakagawa, M., Koyanagi, M., Tanabe, K., Takahashi, K., Ichisaka, T., Aoi, T., Okita, K., Mochiduki, Y., Takizawa, N., and Yamanaka, S. (2008) Generation of induced pluripotent stem cells without Myc from mouse and human fibroblasts. *Nat. Biotechnol.* **26,** 101–106
15. Takahashi, K., Tanabe, K., Ohnuki, M., Narita, M., Ichisaka, T., Tomoda, K., and Yamanaka, S. (2007) Induction of pluripotent stem cells from adult human fibroblasts by defined factors. *Cell* **131,** 861–872
16. Park, I. H., Zhao, R., West, J. A., Yabuuchi, A., Huo, H., Ince, T. A., Lerou, P. H., Lensch, M. W., and Daley, G. Q. (2008) Reprogramming of human somatic cells to pluripotency with defined factors. *Nature* **451,** 141–146
17. Yu, J., Vodyanik, M. A., Smuga-Otto, K., Antosiewicz-Bourget, J., Frane, J. L., Tian, S., Nie, J., Jonsdottir, G. A., Ruotti, V., Stewart, R., Slukvin, I. I., and Thomson, J. A. (2007) Induced pluripotent stem cell lines derived from human somatic cells. *Science* **318,** 1917–1920
18. Meissner, A., Wernig, M., and Jaenisch, R. (2007) Direct reprogramming of genetically unmodified fibroblasts into pluripotent stem cells. *Nat. Biotechnol.* **25,** 1177–1181
19. Aoi, T., Yae, K., Nakagawa, M., Ichisaka, T., Okita, K., Takahashi, K., Chiba, T., and Yamanaka, S. (2008) Generation of pluripotent stem cells from adult mouse liver and stomach cells. *Science* **321,** 699–702
20. Hanna, J., Markoulaki, S., Schorderet, P., Carey, B. W., Beard, C., Wernig, M., Creyghton, M. P., Steine, E. J., Cassady, J. P., Foreman, R., Lengner, C. J., Dausman, J. A., and Jaenisch, R. (2008) Direct reprogramming of terminally differentiated mature B lymphocytes to pluripotency. *Cell* **133,** 250–264
21. Okita, K., Nakagawa, M., Hyenjong, H., Ichisaka, T., and Yamanaka, S. (2008) Generation of mouse induced pluripotent stem cells without viral vectors. *Science* **322,** 949–953
22. Jaenisch, R., and Young, R. (2008) Stem cells, the molecular circuitry of pluripotency and nuclear reprogramming. *Cell* **132,** 567–582
23. Park, I. H., Arora, N., Huo, H., Maherali, N., Ahfeldt, T., Shimamura, A., Lensch, M. W., Cowan, C., Hochedlinger, K., and Daley, G. Q. (2008) Disease-specific induced pluripotent stem cells. *Cell* **134,** 877–886
24. Chang, H., Yoshimoto, M., Umeda, K., Iwasa, T., Mizuno, Y., Fukada, S., Yamamoto, H., Motohashi, N., Miyagoe-Suzuki, Y., Takeda, S., Heike, T., and Nakahata, T. (2009) Generation of transplantable, functional satellite-like cells from mouse embryonic stem cells. *FASEB J.* **23,** 1907–1919
25. Fukada, S., Higuchi, S., Segawa, M., Koda, K., Yamamoto, Y., Tsujikawa, K., Kohama, Y., Uezumi, A., Imamura, M., Miyagoe-Suzuki, Y., Takeda, S., and Yamamoto, H. (2004) Purification and cell-surface marker characterization of quiescent satellite cells from murine skeletal muscle by a novel monoclonal antibody. *Exp. Cell. Res.* **296,** 245–255
26. Baba, S., Heike, T., Umeda, K., Iwasa, T., Kaichi, S., Hiraumi, Y., Doi, H., Yoshimoto, M., Kanatsu-Shinohara, M., Shinohara, T., and Nakahata, T. (2007) Generation of cardiac and endothelial cells from neonatal mouse testis-derived multipotent germline stem cells. *Stem Cell* **25,** 1375–1383
27. Tsuchiya, A., Heike, T., Baba, S., Fujino, H., Umeda, K., Matsuda, Y., Nomoto, M., Ichida, T., Aoyagi, Y., and Nakahata, T. (2007) Long-term culture of postnatal mouse hepatic stem/progenitor cells and their relative developmental hierarchy. *Stem Cell* **25,** 895–902
28. Bulfield, G., Siller, W. G., Wight, P. A., and Moore, K. J. (1984) X chromosome-linked muscular dystrophy (*mdx*) in the mouse. *Proc. Natl. Acad. Sci. U. S. A.* **81,** 1189–1192
29. Harris, J. B. (2003) Myotoxic phospholipases A2 and the regeneration of skeletal muscles. *Toxicon* **42,** 933–945
30. Darabi, R., Gehlbach, K., Bachoo, R. M., Kamath, S., Osawa, M., Kamm, K. E., Kyba, M., and Perlingeiro, R. C. (2008) Functional skeletal muscle regeneration from differentiating embryonic stem cells. *Nat. Med.* **14,** 134–143
31. Bhagavati, S., and Xu, W. (2005) Generation of skeletal muscle from transplanted embryonic stem cells in dystrophic mice. *Biochem. Biophys. Res. Commun.* **333,** 644–649
32. LaBarge, M. A., and Blau, H. M. (2002) Biological progression from adult bone marrow to mononucleate muscle stem cell to multinucleate muscle fiber in response to injury. *Cell* **111,** 589–601
33. Buckingham, M., and Relaix, F. (2007) The role of Pax genes in the development of tissues and organs: Pax3 and Pax7 regulate muscle progenitor cell functions. *Annu. Rev. Cell Dev. Biol.* **23,** 645–673
34. Smith, T. H., Block, N. E., Rhodes, S. J., Konieczny, S. F., and Miller, J. B. (1993) A unique pattern of expression of the four muscle regulatory factor proteins distinguishes somitic from embryonic, fetal and newborn mouse myogenic cells. *Development* **117,** 1125–1133
35. Pownall, M. E., Gustafsson, M. K., and Emerson, C. P., Jr. (2002) Myogenic regulatory factors and the specification of muscle progenitors in vertebrate embryos. *Annu. Rev. Cell Dev. Biol.* **18,** 747–783
36. Barberi, T., Bradbury, M., Dincer, Z., Panagiotakos, G., Socci, N. D., and Studer, L. (2007) Derivation of engraftable skeletal myoblasts from human embryonic stem cells. *Nat. Med.* **13,** 642–648
37. Sakurai, H., Okawa, Y., Inami, Y., Nishio, N., and Isobe, K. (2008) Paraxial mesodermal progenitors derived from mouse embryonic stem cells contribute to muscle regeneration via differentiation into muscle satellite cells. *Stem Cell* **26,** 1865–1873
38. Peault, B., Rudnicki, M., Torrente, Y., Cossu, G., Tremblay, J. P., Partridge, T., Gussoni, E., Kunkel, L. M., and Huard, J. (2007) Stem and progenitor cells in skeletal muscle development, maintenance, and therapy. *Mol. Ther.* **15,** 867–877
39. Ferrari, G., Cusella-De Angelis, G., Coletta, M., Paolucci, E., Stornaiuolo, A., Cossu, G., and Mavilio, F. (1998) Muscle regeneration by bone marrow-derived myogenic progenitors. *Science* **279,** 1528–1530
40. Gussoni, E., Soneoka, Y., Strickland, C. D., Buzney, E. A., Khan, M. K., Flint, A. F., Kunkel, L. M., and Mulligan, R. C. (1999) Dystrophin expression in the *mdx* mouse restored by stem cell transplantation. *Nature* **401,** 390–394
41. Dezawa, M., Ishikawa, H., Itokazu, Y., Yoshihara, T., Hoshino, M., Takeda, S., Ide, C., and Nabeshima, Y. (2005) Bone marrow stromal cells generate muscle cells and repair muscle degeneration. *Science* **309,** 314–317
42. Dellavalle, A., Sampaolesi, M., Tonlorenzi, R., Tagliafico, E., Sacchetti, B., Perani, L., Innocenzi, A., Galvez, B. G., Messina, G., Morosetti, R., Li, S., Belicchi, M., Peretti, G., Chamberlain, J. S., Wright, W. E., Torrente, Y., Ferrari, S., Bianco, P., and Cossu, G. (2007) Pericytes of human skeletal muscle are myogenic precursors distinct from satellite cells. *Nat. Cell Biol.* **9,** 255–267
43. Torrente, Y., Belicchi, M., Sampaolesi, M., Pisati, F., Meregalli, M., D'Antona, G., Tonlorenzi, R., Porretti, L., Gavina, M., Mamchaoui, K., Pellegrino, M. A., Furling, D., Mouly, V., Butler-Browne, G. S., Bottinelli, R., Cossu, G., and Bresolin, N. (2004) Human circulating AC133(+) stem cells restore dystrophin expression and ameliorate function in dystrophic skeletal muscle. *J. Clin. Invest.* **114,** 182–195
44. Sampaolesi, M., Blot, S., D'Antona, G., Granger, N., Tonlorenzi, R., Innocenzi, A., Mognol, P., Thibaud, J. L., Galvez, B. G., Barthelemy, I., Perani, L., Mantero, S., Guttinger, M., Pansarasa, O., Rinaldi, C., Cusella De Angelis, M. G., Torrente, Y., Bordignon, C., Bottinelli, R., and Cossu, G. (2006) Mesoangioblast stem cells ameliorate muscle function in dystrophic dogs. *Nature* **444,** 574–579
45. Hanna, J., Wernig, M., Markoulaki, S., Sun, C. W., Meissner, A., Cassady, J. P., Beard, C., Brambrink, T., Wu, L. C., Townes, T. M., and Jaenisch, R. (2007) Treatment of sickle cell anemia mouse model with iPS cells generated from autologous skin. *Science* **318,** 1920–1923

Received for publication May 20, 2009.
Accepted for publication January 28, 2010.

Journal of Cellular Physiology

Neutrophil Differentiation From Human-Induced Pluripotent Stem Cells

TATSUYA MORISHIMA,[1] KEN-ICHIRO WATANABE,[1] AKIRA NIWA,[2] HISANORI FUJINO,[1] HIROSHI MATSUBARA,[1] SOUICHI ADACHI,[1] HIROFUMI SUEMORI,[3] TATSUTOSHI NAKAHATA,[2] AND TOSHIO HEIKE[1]*

[1]*Department of Pediatrics, Graduate School of Medicine, Kyoto University, Kyoto, Japan*

[2]*Department of Clinical Application, Center for iPS Cell Research and Application, Kyoto University, Kyoto, Japan*

[3]*Laboratory of Embryonic Stem Cell Research, Stem Cell Research Center, Institute for Frontier Medical Sciences, Kyoto University, Kyoto, Japan*

Induced pluripotent stem (iPS) cells are of potential value not only for regenerative medicine, but also for disease investigation. The present study describes the development of a neutrophil differentiation system from human iPS cells (hiPSCs) and the analysis of neutrophil function and differentiation. The culture system used consisted of the transfer of hiPSCs onto OP9 cells and their culture with vascular endothelial growth factor (VEGF). After 10 days, TRA 1-85^{+}CD34^{+}VEGF receptor-2 (VEGFR-2)^{high} cells were sorted and co-cultured with OP9 cells in the presence of hematopoietic cytokines for 30 days. Floating cells were collected and subjected to morphological and functional analysis. These hiPSC-derived neutrophils were similar to peripheral blood mature neutrophils in morphology, contained functional neutrophil specific granules, and were equipped with the basic functions such as phagocytosis, superoxide production, and chemotaxis. In the process of differentiation, myeloid cells appeared sequentially from immature myeloblasts to mature segmented neutrophils. Expression patterns of surface antigen, transcription factors, and granule proteins during differentiation were also similar to those of granulopoiesis in normal bone marrow. In conclusion, differentiation of mature neutrophils from hiPSCs was successfully induced in a similar process to normal granulopoiesis using an OP9 co-culture system. This system may be applied to elucidate the pathogenesis of various hematological diseases that affect neutrophils.

J. Cell. Physiol. 226: 1283–1291, 2011.

Neutrophils and/or myeloid differentiation are most commonly affected in various hematological diseases including inherited bone marrow failure syndromes and neutrophil function disorders. Responsible genes have been identified in most of these syndromes or diseases, but the association between the gene mutation and the specific phenotype is not always clear. Moreover, often patients who present with a specific syndrome lack mutations in the known genes (Alter, 2007). Understanding the pathophysiology of these syndromes has been challenging despite the information provided by recent molecular findings, and in many of these syndromes, experimental models have not yet been generated.

Murine models of human congenital and acquired diseases are invaluable for disease investigation, but they provide a limited representation of human pathophysiology because they often do not faithfully mimic human diseases. The differences between murine and human physiologies make human cell culture an essential complement to research with animal models of disease.

Induced pluripotent stem (iPS) cells are reprogrammed somatic cells with embryonic stem (ES) cell-like characteristics generated by the introduction of combinations of specific transcription factors (Takahashi and Yamanaka, 2006; Meissner et al., 2007; Okita et al., 2007; Takahashi et al., 2007; Yu et al., 2007; Park et al., 2008b). Given the robustness of the approach, direct reprogramming promises to be a facile source of patient-derived cell lines. Such lines would be immediately valuable not only for regenerative medicine, but for disease investigation and drug screening as well.

The pluripotency and self-renewal potential of ES cells contributes to their value in various fields of science (Evans and Kaufman, 1981). Previous studies using normal or gene-manipulated ES cells have helped elucidate the process of normal embryogenesis and the genetic mechanisms of certain diseases (Lensch and Daley, 2006; Tulpule et al., 2010). Use of human embryos, however, faces ethical controversies that hinder the applications of human ES cells (hESCs). In addition, it is difficult to generate patient- or disease-specific ES cells, which are required for their effective application. The use of iPS cells would avoid the controversies surrounding human embryonic stem cell research.

Patient-specific iPS cells can be used for the generation of disease-corrected, patient-specific cells for cell therapy applications. Disease-specific pluripotent cells capable of differentiation into the various tissues affected in each condition can also provide new insights into disease pathophysiology by permitting analysis in a human system, under controlled conditions in vitro. Recent studies reported the generation of disease-specific iPS cell lines from patients with a variety of diseases (Park et al., 2008a; Raya et al., 2009; Agarwal et al., 2010). Therefore, disease-specific iPS cells are expected to be good models for the investigation of different diseases, and

Contract grant sponsor: The Ministry of Education, Culture, Sports, Science and Technology, Japan.

*Correspondence to: Toshio Heike, Department of Pediatrics, Graduate School of Medicine, Kyoto University, 54 Kawahara-cho, Shogoin, Sakyo-ku, Kyoto 606-8507, Japan.
E-mail: heike@kuhp.kyoto-u.ac.jp

Received 21 May 2010; Accepted 20 September 2010

Published online in Wiley Online Library (wileyonlinelibrary.com), 13 October 2010.
DOI: 10.1002/jcp.22456

effective neutrophil differentiation systems are required to investigate the pathogenesis of various hematological conditions that affect neutrophils using human iPS cells (hiPSCs).

Recent reports describe in vitro culture systems for neutrophil differentiation from hESCs (Choi et al., 2009; Saeki et al., 2009; Yokoyama et al., 2009); however, neutrophil differentiation from hiPSCs has not yet been reported in detail. One of these studies demonstrated that myeloid differentiation could be induced from hiPSCs using the same methodology employed for their differentiation from hESCs (Choi et al., 2009), but the differentiation process and the functions of hiPSC-derived neutrophils were not shown in detail. A system for erythroid differentiation from primate ES and murine iPS cells by co-culture with OP9 stromal cells was developed in previous studies (Umeda et al., 2004; Umeda et al., 2006; Shinoda et al., 2007; Niwa et al., 2009). In the present study, a neutrophil differentiation system from hiPSCs was established by modifying the erythroid differentiation system, and the functions of the hiPSC-derived neutrophils and their differentiation process were analyzed in detail. This system may contribute to the elucidation of the pathogenesis of various blood diseases and the development of novel therapeutic approaches.

Materials and Methods

Maintenance of cells

The human iPS cell lines 201B6, 253G1 and 253G4 were a kind gift from Dr. Yamanaka (Kyoto University, Kyoto), and were generated from human dermal fibroblasts by retrovirus-mediated transfection of four (201B6) or three (253G1 and 253G4) transcription factors (Oct3/4, Sox2, and Klf4, with or without c-Myc) (Takahashi et al., 2007; Nakagawa et al., 2008). The human iPS cell lines and the human ES cell line KhES3-EGFPneo (KhES-3G) were maintained on mitomycin-C (Kyowa Hakko Kirin, Tokyo, Japan) -treated mouse embryonic fibroblasts (MEFs) in DMEM/F12 (Sigma-Aldrich, St. Louis, MO) supplemented with 20% Knockout™ Serum Replacement (Invitrogen, Carlsbad, CA), 5 ng/ml basic fibroblast growth factor (bFGF; R&D Systems, Minneapolis, MN), 1% non-essential amino acids solution (Invitrogen), 5 mM sodium hydroxide solution, 100 μM 2-mercaptethanol, and 2 mM L-glutamine. The culture medium was replaced daily with fresh medium. Colonies were passaged onto new MEFs every 3 or 4 days. The human ES cell line was used in conformity with The Guidelines for Derivation and Utilization of Human Embryonic Stem Cells of the Ministry of Education, Culture, Sports, Science, and Technology, Japan. OP9 stromal cells, which were a kind gift from Dr. Kodama (Osaka University, Osaka), were maintained in α-MEM (Invitrogen) supplemented with 20% fetal calf serum (FCS; Biological Industries, Bet Haemek, Israel).

Antibodies

The antibodies used for flow cytometric analysis included fluorescein isothiocyanate (FITC)-conjugated anti-human TRA 1-85 (R&D Systems), CD45 (Becton-Dickinson, Franklin Lakes, NJ) antibodies, phycoerythrin (PE)-conjugated anti-human CD11b, CD34 (Beckman Coulter, Fullerton, CA), CD13, CD16, CD33 (Becton-Dickinson) antibodies, and allophycocyanin (APC)-conjugated anti-human vascular endothelial growth factor receptor-2 (VEGFR-2) (eBioscience, San Diego, CA) antibody. The primary antibodies used for immunocytochemical analysis included goat anti-human lactoferrin (Santa Cruz Biotechnology, Santa Cruz, CA) and rabbit anti-human MMP9 (Abcam, Cambridge, UK). Biotinylated horse anti-goat or anti-rabbit antibodies (Vector Laboratories, Burlingame, CA) were used as secondary antibodies.

Differentiation of iPS cells

Methods used for the initial differentiation of iPS cells and cell sorting were based on earlier reports (Umeda et al., 2004, 2006). Briefly, trypsin-treated undifferentiated iPS cells were transferred onto OP9 cells and cultured with 20 ng/ml vascular endothelial growth factor (VEGF) (R&D Systems). After 10 days, the induced cells were harvested with cell dissociation buffer (Invitrogen), and sorted TRA 1-85^{+}CD34^{+}VEGFR-2^{high} cells were transferred onto fresh OP9 cells in six-well plates at a concentration of 3×10^{3} cells per well. Sorted cells were cultured in α-MEM (Invitrogen) containing 10% FCS (Sigma, St Louis, MO), 50 μM 2-mercaptoethanol, 20 ng/ml interleukin (IL)-3, 100 ng/ml stem cell factor (SCF) (R&D Systems), and 10 ng/ml thrombopoietin (TPO) for 20 days. On day 20 after cell sorting, cytokines were changed into 20 ng/ml IL-3 and 10 ng/ml granulocyte colony-stimulating factor (G-CSF). IL-3, TPO and G-CSF were kindly provided by Kyowa Hakko Kirin.

Flow cytometric analysis and cell sorting

Cells were trypsinized and stained with antibodies. Dead cells were excluded by 4',6-diamidino-2-phenylindole (DAPI) staining. Samples were analyzed using an LSR flow cytometer and Cell Quest software (Becton Dickinson). Cell sorting was performed using a FACSVantage SE flow cytometer (Becton Dickinson).

Cytostaining

Floating cells were centrifuged onto glass slides using a Shandon Cytospin® 4 Cytocentrifuge (Thermo, Pittsburgh, PA), and analyzed by microscopy after May–Giemsa, myeloperoxidase (MPO), or alkaline-phosphatase staining. Sequential morphological analysis was performed as follows: all adherent cells including OP9 cells were trypsinized, harvested, and incubated in a new tissue-culture dish (Becton-Dickinson) for 1 h to eliminate adherent OP9 cells (Suwabe et al., 1998). Floating cells were then collected, centrifuged onto glass slides, and analyzed by microscopy after May–Giemsa staining. For immunocytochemical analysis, cells were fixed with 4% paraformaldehyde (PFA), immersed in citrate buffer, and autoclaved for 5 min at 121°C for antigen retrieval (Toda et al., 1999). The slides were then incubated with primary antibodies followed by application of the streptavidinbiotin complex immunoperoxidase technique with diaminobenzidine as chromogen, and nuclei were counterstained with hematoxylin.

Electron microscopy

Cells were fixed in 2% glutaraldehyde in 0.1 M phosphate buffer (PB) for at least 2 h, and then postfixed in 1% osmium tetroxide in 0.1 M PB for 1.5 h. After fixation, samples were dehydrated in a graded ethanol series, cleared with propylene oxide, and embedded in Epon. Thin sections of cured samples were stained with uranyl acetate and Reynolds lead citrate. The sections were inspected using a transmission electron microscope, H7650 (Hitachi, Tokyo, Japan).

Chemotaxis assay

Chemotactic ability was determined using a modified Boyden chamber method (Boyden, 1962; Harvath et al., 1980). Briefly, 500 μl of the reaction medium (Hank's Balanced Salt Solution (HBSS) containing 2.5% FCS) with or without 10 nM formyl-Met-Leu-Phe (fMLP; Sigma-Aldrich) was placed into each well of a 24-well plate, and the cell culture insert (3.0-μm pores; Becton Dickinson) was gently placed into each well to divide the well into upper and lower sections. Floating cells were suspended in the reaction medium at 7.0×10^{4}/ml, and a 500-μl cell suspension was added to the upper well, allowing the cells to migrate from the upper to the lower side of the membrane for 4 h at 37°C. After incubation, cells in the lower chamber were collected and counted using an LSR flow cytometer. Cells were counted by flow cytometry as follows:

equivalent amounts of counting beads were added to each sample and counted until the bead count reached 10,000.

MPO activity assay

The EnzChek Myeloperoxidase (MPO) Activity Assay Kit (Molecular Probes, Leiden, The Netherlands) was used for rapid and sensitive determination of MPO chlorination activity in cell lysates. The procedure was performed following the manufacturer's instructions. Cell lysate samples were prepared from 1×10^4 floating cells by freeze-thaw cycles. Fluorescence was measured with a fluorescence microplate reader (Wallac 1420 ARVO sx; PerkinElmer, Waltham, MA) using fluorescence excitation and emission at 485 and 530 nm, respectively. The background fluorescence measured for each zero-MPO control reaction was subtracted from each fluorescence measurement before plotting.

DHR assay

Neutrophil production of reactive oxygen species was detected by flow cytometry using dihydrorhodamine123 (DHR) as described previously (Vowells et al., 1995). Briefly, 3.5×10^4 floating cells were suspended in 100 μl of the reaction buffer (HBSS containing 0.1% FCS and 5 mM glucose) per tube, and two tubes were prepared for each sample. Catalase (Sigma-Aldrich) at a final concentration of 1000 U/ml and DHR at a final concentration of 1.0×10^5 nM were added and incubated for 5 min in a 37°C shaking water bath. After incubation, phorbol myristate acetate (PMA; Sigma-Aldrich) at a final concentration of 400 ng/ml was added to one of the two tubes and tubes were returned to the water bath for an additional 15 min. Following incubation, rhodamine fluorescence from the oxidized DHR was detected using an LSR flow cytometer.

Phagocytosis and detection of reactive oxygen species

Phagocytosis and neutrophil production of reactive oxygen species was detected by chemiluminescent microspheres (luminol-binding carboxyl hydrophilic microspheres; TORAY, Tokyo, Japan) as described previously (Uchida et al., 1985). Briefly, 2×10^4 floating cells were suspended in 50 μl of the reaction buffer (HBSS containing 20 mM N-2-hydroxyethylpiperazine-N′-2-ethanesulfonic acid (HEPES)) per tube. To activate the system, 5 μl of chemiluminescent microspheres was added, and light emission was recorded continuously. During the measurement, samples were kept at 37°C. To inhibit the phagocytosis, 1.75 μg of cytochalasin B (Sigma-Aldrich) was added to the sample. Chemiluminescence from the microspheres was detected using a luminometer (TD-20/20; Turner Designs, Sunnyvale, CA).

RNA extraction and RT-PCR analysis

RNA samples were prepared using silica gel membrane-based spin-columns (RNeasy Mini-Kit™, Qiagen, Valencia, CA) and subjected to reverse transcription (RT) with the Ominscript-RT Kit™ (Qiagen). All procedures were performed following the manufacturer's instructions. For reverse transcriptase-polymerase chain reaction (RT-PCR), yields were adjusted by dilution to produce equal amounts of the human glyceraldehyde-3-phosphate dehydrogenase (GAPDH) amplicon. The complementary DNA (cDNA) templates were initially denatured at 94°C for 5 min, followed by 30–40 amplification reactions consisting of 94°C for 15–30 sec (denaturing), 55–63°C for 15–30 sec (annealing), and 72°C for 30–60 sec (extension), with a final extension at 72°C for 7 min. The oligonucleotide primers were as follows: NANOG, 5′-CAG CCC TGA TTC TTC CAC CAG TCC C-3′ and 5′-TGG AAG GTT CCC AGT CGG GTT CAC C-3′ (Takahashi et al., 2007); human GAPDH, 5′-CAC CAG GGC TGC TTT TAA CTC TG-3′ and 5′-ATG GTT CAC ACC CAT GAC GAA C-3′ (Umeda et al., 2006); PU.1, 5′-CTG CAT TGG CCC CCA CCG AG-3′ and 5′-AGG TCT TCT GAT GGC TGA GGG GG-3′; C/EBPα, 5′-TAA CCT TGT GCC TTG GAA ATG CAA AC-3′ and 5′- ATG TTT CCA CCC CTT TCT AAG GAC A-3′ (Duan and Horwitz, 2003); C/EBPε, 5′- AGT CTG GGG AAG AGC AGC TTC-3′ and 5′- ACA GTG TGC CAC TTG GTA CTG-3′ (Mori et al., 2009); MPO, 5′-TGA GGA CGG CTT CTC TCT TC-3′ and 5′-CCC GGT AAG TGA TGA TCT GG-3′; Lactoferrin, 5′-AGC TGG CAG ACT TTG CGC T-3′ and 5′-TTC AGA TTA GTA ATG CCT GCG ACA TAC-3′ (Kholodnyuk et al., 2006); Gelatinase (MMP-9), 5′-GCC TCC AAC CAC CAC CAC AC-3′ and 5′-GCC CAG CCC ACC TCC ACT C-3′ (Sugimoto et al., 2001); mouse GAPDH, 5′-ACG GCC GCA TCT TCT TGT GCA-3′ and 5′-CAC CCT TCA AGT GGG CCC CG-3′. PCR amplification reaction cycles were performed in the linear range for each primer by carrying out primer titrations. The number of reaction cycles per sample were: NANOG, 35 cycles; human GAPDH, 30 cycles; PU.1, 40 cycles; C/EBPα, 40 cycles; C/EBPε, 40 cycles; MPO, 35 cycles; Lactoferrin, 35 cycles; Gelatinase (MMP-9), 40 cycles; mouse GAPDH, 30 cycles.

Statistics

Statistical analyses were conducted using the Student's *t*-test. Statistical significance was defined as $P < 0.05$.

Results

Neutrophil differentiation from hiPSCs in co-culture with OP9 stromal cells

A culture system for the induction of erythroid cell differentiation from primate ES and murine iPS cells by co-culture with OP9 stromal cells (Umeda et al., 2004; Umeda et al., 2006; Shinoda et al., 2007; Niwa et al., 2009) was established, and this system was applied for neutrophil differentiation from hiPSCs. Prior data in primate ES cells suggested that the VEGFR-2^{high} fraction of differentiated cells contained hemangioblasts and VEGFR-2^{high}CD34$^+$ cells had more hematopoietic potential (Umeda et al., 2006). Therefore, the expression of VEGFR-2 and CD34 was examined using three human iPS cell lines (201B6, 253G1, 253G4) and one ES cell line (KhES-3G). After 10 days of co-culture with OP9 in the presence of 20 ng/ml VEGF, VEGFR-2^{high}CD34$^+$ cells appeared from all hiPSC lines in a similar manner to the ES cell line (Fig. 1A). Among these three human iPS cell lines, the highest percentage of VEGFR-2^{high}CD34$^+$ cells was detected in 253G4 (Fig. 1B), and the data on this cell line is therefore presented below.

The VEGFR-2^{high}CD34$^+$ cell fraction was sorted (Fig. 1C) and 1.1×10^4 (range; 0.6–2.2×10^4 in 14 independent cultures) VEGFR-2^{high}CD34$^+$ cells were grown in one 10-cm dish containing hiPSCs. They were then transferred onto fresh OP9 cells and cultured in the presence of hematopoietic cytokines. Around 10 days after cell sorting (day10 + 10), small, round cell colonies appeared (Fig. 1D), and these colonies gradually grew in both size and number (Fig. 1E). At the same time, floating cells also appeared, and the average number of floating cells from 1×10^4 sorted VEGFR-2^{high}CD34$^+$ cells at 30 days after cell sorting (day10 + 30) was 4.1×10^4 (range; 0.2–9.9×10^4 in 11 independent cultures).

May–Giemsa staining of the floating cells on day 10 + 30 revealed that 38.0 ± 1.6% of the cells were stab and segmented neutrophils (Fig. 1F), which were positive for MPO (Fig. 1G) and neutrophil alkaline-phosphatase (Fig. 1H). The rest were mainly immature myeloid cells and a small number of macrophages, and cells of other lineages, such as erythroid or lymphoid cells, were not observed. The frequency of MPO- and neutrophil alkaline-phosphatase-positive cells is shown in Table 1. The results were consistent with the morphological features revealed by May–Giemsa staining.

Surface marker analysis revealed that these floating cells were positive for CD45 and CD11b, and partially positive for CD13, CD33, and CD16 (Fig. 1I). The expression pattern of these surface markers was similar to that of neutrophils or immature myeloid cells in healthy bone marrow (van Lochem et al., 2004), although the CD16 expression level was lower.

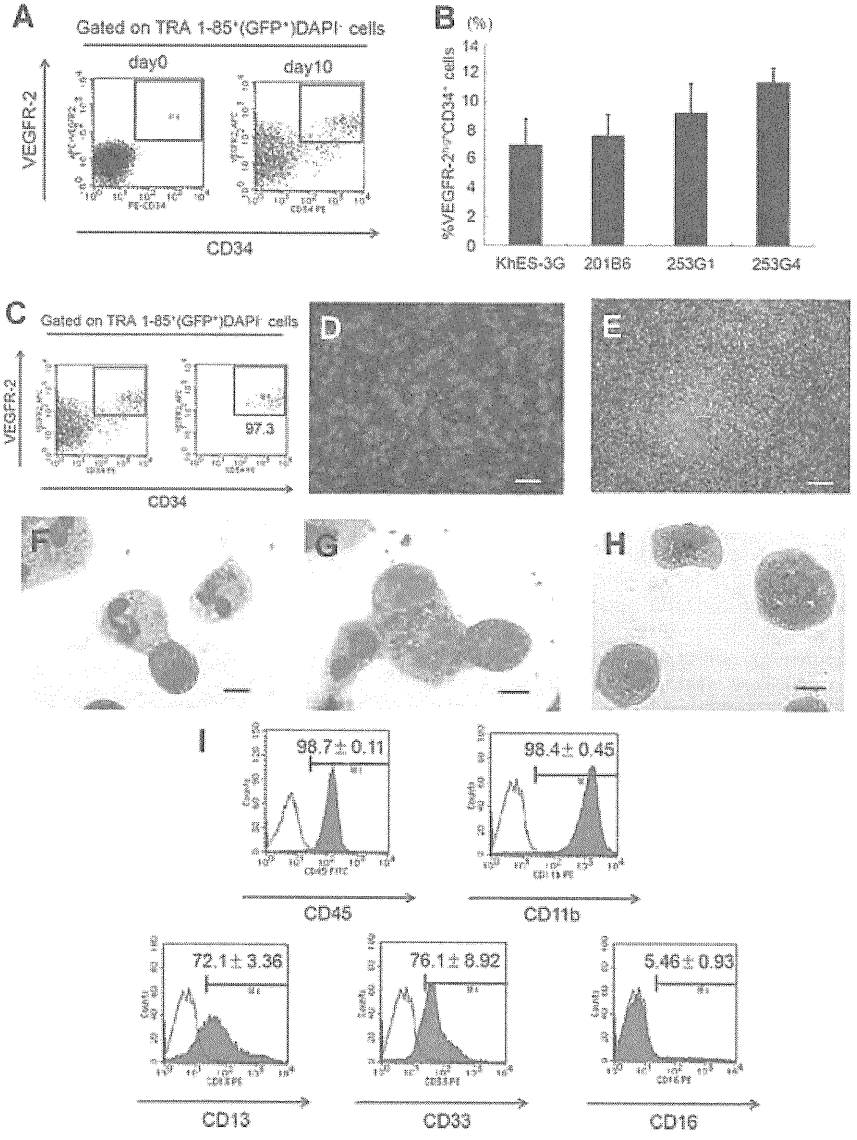

Fig. 1. Neutrophil differentiation from hiPSCs in co-culture with OP9 stromal cells. (A–B) Flow cytometric analysis of VEGFR-2 and CD34 during differentiation induction. TRA 1-85$^+$ (GFP$^+$) DAPI$^-$ cells were gated as human iPS (ES) cell-derived viable cells. Undifferentiated iPS (ES) cells and 10-day culture cells were stained with antibodies specific for VEGFR-2 and CD34. Representative results from one of three independent experiments (A) and percentages of VEGFR-2^{high}CD34$^+$ cells on day 10 (B) are shown (n = 3; bars represent SDs). (C) VEGFR-2^{high}CD34$^+$ cells were sorted on day 10. Representative dot plots and percentages of gated cells are shown. Purities of viable VEGFR-2^{high}CD34$^+$ cells were calculated at 95.5 ± 1.9% from 14 independent experiments. (D–E) Micrographs of adherent hematopoietic cell clusters generated on day 10 (D) and day 30 (E) after cell sorting. Scale bars: 200 μm. (F–H) May–Giemsa staining (F), myeloperoxidase staining (G), and neutrophil alkaline-phosphatase staining (H) of floating cells on day 10 + 30. Scale bars: 10 μm. (I) Flow cytometric analysis of floating cells on day 10 + 30 were stained with antibodies specific for CD45, CD11b, CD13, CD33, or CD16. Plots show the negative control profile (open bars) versus the specific antibody staining profiles (shaded bars). Representative results from one of three independent experiments are shown. [Color figure can be viewed in the online issue, which is available at wileyonlinelibrary.com.]

TABLE 1. Frequency of staining-positive cells for neutrophil specific granules

Staining	Frequency of positive cells (%)
Myeloperoxidase	93.7 ± 1.7
Neutrophil alkaline-phosphatase	39.0 ± 2.2
Lactoferrin	79.0 ± 1.4
Gelatinase	59.0 ± 3.7

Data are shown as mean ± SD (n = 3 independent experiments).

This lower CD16 expression level was similar to that of neutrophils derived in vitro from bone marrow CD34$^+$ cells by stimulation with G-CSF (Kerst et al., 1993b) and to the effect in vivo when G-CSF is administered to healthy volunteers (Kerst et al., 1993a). These results indicated that the modified OP9 co-culture system could differentiate mature neutrophils from immature hiPSCs.

hiPSC-derived neutrophils contain neutrophil specific granules

Mature neutrophils in vivo have intracellular granules that are important for their bactericidal function. The granules can be

classified into three types based on their size, morphology, or electron density, or with reference to a given protein: primary (azurophilic) granules contain MPO, secondary granules contain lactoferrin, and tertiary granules contain gelatinase (Borregaard and Cowland, 1997).

To assess the presence of these granules in hiPSC-derived neutrophils, they were imaged using transmission electron microscopy, which showed that the hiPSC-derived mature neutrophils contained peroxidase-positive and negative granules, as was observed in peripheral blood neutrophils (Fig. 2A–B). Immunocytochemical analysis revealed that hiPSC-derived mature neutrophils were also positive for lactoferrin and gelatinase (Fig. 2C–D). The frequencies of cells that were positive for neutrophil specific granules, as observed by transmission electron microscopy (Table 2) and immunocytochemical analysis (Table 1), were more than 90% for primary granules, about 80% for secondary granules, and approximately 60% for tertiary granules. These results indicated that hiPSC-derived neutrophils contained neutrophils-specific granules.

hiPSC-derived neutrophils exhibit biological bactericidal activities

Because neutrophils patrol circulating blood and play a key role in early phase defense mechanisms, the chemotactic, phagocytotic, and bactericidal activities of hiPSC-derived neutrophils were analyzed.

Chemotactic activity was assessed using a modified Boyden chamber method (Boyden, 1962; Harvath et al., 1980). After incubation with or without fMLP in the lower well, neutrophils had migrated from the upper side to the lower side of the membrane. Incubation with fMLP caused an increase in the number of migrated cells of more than three times compared to cells without fMLP, suggesting that hiPSC-derived neutrophils had chemotactic activity in response to a chemoattractant similar to natural neutrophils derived from bone marrow (Fig. 3A).

The MPO-dependent chlorination activity and reactive oxygen production of hiPSC-derived neutrophils, which are

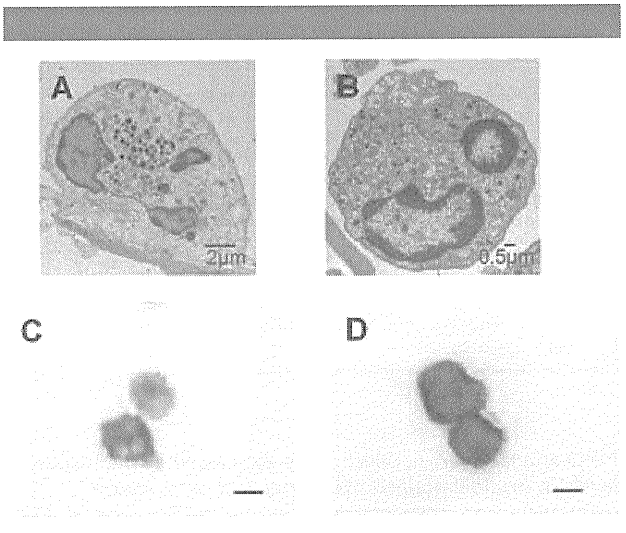

Fig. 2. Neutrophil-specific granules in hiPSC-derived neutrophils. (A–B) Floating cells on day10 + 30 (A) and peripheral blood neutrophils (B) were analyzed by transmission electron microscope. (C–D) Immunocytochemical analysis. Floating cells on day10 + 30 were stained for lactoferrin (C) and MMP9 (gelatinase) (D). Scale bars: 10 μm. [Color figure can be viewed in the online issue, which is available at wileyonlinelibrary.com.]

TABLE 2. Frequency of positive cells for neutrophil specific granules under transmission electron microscopy

Granules	Frequency of positive cells (%)
Peroxidase-positive granules	95.1 (135/142)
Peroxidase-negative granules	86.6 (123/142)

both essential for their bactericidal function, were determined next. MPO reacts with hydrogen peroxide (H_2O_2) to form the active redox and enzyme intermediate compound MPO-I, which oxidizes chloride (Cl^-) to HOCl (Winterbourn, 2002). As shown in Figure 3B, hiPSC-derived neutrophils showed MPO-dependent chlorination activity. To evaluate reactive oxygen production, the ability to convert DHR to rhodamine was assessed using flow cytometry (Vowells et al., 1995) and the results revealed that hiPSC-derived neutrophils characteristically produced superoxide in response to PMA (Fig. 3C).

Finally, phagocytotic activity and phagosome-dependent reactive oxygen production were measured using luminol-bound microspheres (Uchida et al., 1985). As shown in Figure 3D, the captured data confirmed that hiPSC-derived neutrophils could produce reactive oxygen species in response to the phagocytosis of microspheres, which was completely abolished in the presence of the antiphagocytic agent cytochalasin B. Moreover, transmission electron microscopy successfully captured a screenshot of a neutrophil phagocytosing the microbeads (Fig. 3E). The above results clearly show that neutrophils derived from hiPSC using the present culture system maintain their functional status.

Step-wise neutrophil differentiation from hiPSCs is similar to normal granulopoiesis

Disorders of neutrophil differentiation are observed in various hematological diseases, among them the maturation arrest of neutrophil precursors in the bone marrow at the promyelocyte stage in severe congenital neutropenia. Thus, in clinical applications for disease investigation, the sequential analysis of the differentiation process from hiPSC to mature neutrophils in this culture system is required.

Observation of the sequential changes in cell morphology was done using May–Giemsa staining. Visualization of the morphology of day10 + 10 cells revealed that the cells were mainly myeloblasts and promyelocytes (Fig. 4A). On day10 + 20, myelocytes and metamyelocytes became predominant (Fig. 4B), and on day 10 + 30, stab and segmented neutrophils became predominant (Fig. 4C).

Surface antigen expression at each differentiation stage of hiPSC-derived cells was analyzed by flow cytometry (Fig. 4D). CD34, cell surface marker on normal immature hematopoietic cells, was detected in about 20% of the cells on day 10 + 10, but disappeared gradually thereafter. From day 10 + 10 to 10 + 30, the common myeloid antigens CD11b and CD33 were expressed in almost all the cells. Interestingly, expression of CD13, also a common myeloid antigen, was observed in less than 20% of cells at day 10 + 10 and did not subsequently increase. The expression level of CD16, which is a representative marker of matured neutrophils (van de Winkel and Anderson, 1991), doubled from day 10 + 10 to day 10 + 20, although the increase in expression was not statistically significant. These expression patterns were consistent with the patterns observed during normal neutrophil differentiation in healthy bone marrow (van Lochem et al., 2004).

The gene expression patterns of the pluripotency marker, transcription factors and granule proteins during neutrophil